FISEVIER

Contents lists available at ScienceDirect

Progress in Surface Science

journal homepage: www.elsevier.com/locate/progsurf



Review article

Plasmonic decay into hot electrons in silver

Hrvoje Petek ^{a,*}, Andi Li ^a, Xintong Li ^b, Shijing Tan ^b, Marcel Reutzel ^c

- ^a Department of Physics and Astronomy and the IQ Initiative, University of Pittsburgh, Pittsburgh, PA 15260, USA
- b Hefei National Research Center for Physical Sciences at the Microscale, University of Science and Technology of China, Hefei, Anhui 230026, China
- ^c I. Physikalisches Institut, Georg-August-Universität Göttingen, Göttingen 37077, Germany

ARTICLE INFO

Commissioning Editor: Aart Kleyn

ABSTRACT

Light at optical frequencies interacting with a metal surface can excite interband quantum transitions, or intraband currents at frequencies approaching the PHz range. Momentum conservation enables the interband excitation to occur in first order as a dipole transition, while intraband excitations involve second-order momentum scattering processes. The free electron response to optical fields can also be collective, causing the optical field to be screened by the multipole plasmon response. We describe the exitation of single crystal silver surfaces in the region where the dielectric response transits from negative to positive passing through the epsilon near zero (ENZ) condition. There, electrons can no longer screen the optical field, so that it penetrates as a collective charge density wave of the free electron plasma, in other words, as a bulk transverse or longitudinal plasmon field. We examine two-photon photoemission (2PP) signals from Ag(111), (100) and (110) surfaces through the ENZ region under conditions where intraband, and interband single particle, and bulk plasmon collective responses dominate. We are specifically interested in the bulk plasmon decay into plasmonic photoemission. Plasmonic decay into excitation of electrons from the Fermi level, which we observe as a nonlinear 2PP process, has been established for the free electron and noble metals, but its significance to transduction of optical-to-electronic energy has not penetrated the plasmonics community. 2PP spectra show evidence for intraband hot electron generation, interband surface and bulk band excitation, and nonlinear bulk plasmon driven plasmonic single particle excitation. Because the intraband and plasmonic decay into hot electron distributions have been extensively considered in the literature, without reference to explicit experimental measurements, we discuss such processes in light of the directional anisotropy of the electronic structure of single crystalline silver. We note that projected band gaps in silver exclude large regions of the unoccupied state density from hot electron generation, such that it predominantly occurs in the (110) direction. Moreover, the excited hot electron distributions do not follow expectations from the joint density of the occupied and unoccupied states of a free electron metal, as assumed in majority of research on hot electron processes. We describe the strongly anisotropic hot electron distributions recorded by 2PP spectroscopy of Ag surfaces, and the plasmonic photoemission process that occurs on all surfaces

Abbreviations: TR-mPP, time resolved multiphoton photoemission (spectroscopy); AR-mPP, angle resolved multiphoton photoemission (spectroscopy); LP, localized plasmons; 2PP, two-photon photoemission; mPP, multi-photon photoemission (m=2–10); ENZ, epsilon (dielectric constant) near zero; SPP, surface plasmon polariton; SAM, spin angular momentum; OAM, orbital angular momentum; ITR-PEEM, interferometric time-resolved photoemission electron microscopy; SS, Shockley surface state; IP1, Image potential state (n=1); L_{sp} , lower sp-band; U_{sp} , upper sp-band; E_{F} , Fermi level; E_{V} , vacuum level; TS, Tamm surface state; $\hbar\omega_{L}$, laser photon energy; ITR-2PP, interferometric time-resolved two photon photoemission; FT, Fourier transform; $E_{f}(k_{\parallel})$, Final state energy vs. parallel momentum (spectra); ω_{p} , bulk plasmon frequency.

E-mail address: petek@pitt.edu (H. Petek).

https://doi.org/10.1016/j.progsurf.2023.100707

^{*} Corresponding author.

irrespective of the momentum-dependent single particle band structure of silver. Plasmonic photoemission, or its linear analog that excites hot electrons at energies below the work function of Ag, is an important process for harvesting hot electron energy in photocatalytic and electronic device applications because the plasmon energy is not distributed between an electron and hole. This plasmonic decay channel is robust, but many aspects raise further questions. The accompanying publication by Gumhalter and Novko discusses the plasmonic photoemission from a theoretical point of view and its extension to Floquet engineering, as an exploration of novel plasmonic excitation processes in metals.

1. Introduction

Illumination of metals by optical fields can drive collective plasmonic or single particle intraband and interband responses that ultimately terminate in single particle, so called, hot electron [1-24] excitations. Much research has been devoted to the excitation of the spectroscopically bright plasmonic modes, which typically decay on < 10 fs time scales into hot electrons (and potentially holes) that are thought to subsequently activate photocatalytic or photovoltaic processes. In such experiments, one can easily define and correlate the electromagnetic response that is optically driven and the chemical products or photovoltages that are created, but details of the energy transduction remain a topic of untested interpretation; one often invokes intermediate hot electron excitation without much knowledge of their energy and momentum distributions, or their lifetimes, which are essential to define and optimize the efficiency of processes that are attributed to them. We wish to shed light on the black box of hot electron generation for the purpose of guiding the discussion and research that might illuminate photon energy transduction in metallic systems [25–27]. We first discuss hot electron energy and momentum distributions from the perspective of one- or two-color time and angle resolved multiphoton photoemission (TR-mPP; AR-mPP) spectroscopy [2,28–38], which is in principle capable of defining the primary hot electron distributions and their relaxation on femtosecond time scale. Specifically, we focus on mPP spectroscopy [39,40] of single crystal silver surfaces [41-46]. We next describe the single particle features due to interband and intraband electron excitations. This forms the basis for finally discussing plasmonic photoemission, which we describe as non-Einsteinian 2PP process, where the bulk plasmon at a frequency defined by the electron density and mass, rather than the excitation frequency, decays to excite photoelectrons specifically from the Fermi level, E_F , rather than democratically according to a free electron density of states (**DOS**) from a range of initial $E_F - \hbar \omega$ to final $E_F + \hbar \omega$ states, as is broadly assumed [13,15,24]. The plasmonic photoemission that we report [41–46] i) is in line with linear spectroscopic photoemission measurements of simple metals [47,48]; ii) is predicted by ab initio theory [49]; and iii) has been reported as a linear process for Ag surfaces with reduced work functions [50,51]. This process is particularly relevant to energy transduction in photocatalytic processes, because the entire plasmon energy is transferred to hot electrons, rather than being divided between the photohole and hot electron. In conjunction with the theory article by Gumhalter and Novko [52], we aim to familiarize the reader with the concept of plasmonic photoemission, and its implications on plasmonic hot electron generation in metals.

In this review, we first introduce the collective response modes of free electron plasmas, that are colloquially called plasmons, but differ in their dimensionality and localization. We recommend the following articles on the theory of collective plasmonic electron responses to optical fields and charged particles, which provide accessible introduction into plasmon physics [6,53–55].

The fundamental collective response of a free electron plasma to optical fields is described by the classical Drude dielectric function, $\epsilon(\omega)$, which also includes contributions from the bound electrons, ϵ_b :

$$\epsilon(\omega) = \epsilon_b - \omega_p^2 / \omega^2. \tag{1}$$

The bulk plasmon frequency, or the longitudinal plasmon, represented by ω_p depends on the free electron density, N, and electron mass, m_e , as,

$$\omega_p = \sqrt{4\pi N e^2/m_e}. ag{2}$$

In free electron and noble metals, ω_p is in the 2–18 eV [56–58] and 2–4 eV range, respectively [59,60]. Although transition metals are not considered plasmonic, they have plasmonic responses that are strongly damped by facile hot electron excitation in the d-bands that cross the Fermi level [61]. The plasmonic responses can be further delineated as nondispersive longitudinal and dispersive transverse responses, ω_t . They are related by:

$$\omega_t^2 = \omega_p^2 + c^2 k^2 \tag{3}$$

where c and k are the speed of light and momentum [55,62]. Our primary focus is on Ag, for which $\omega_p \sim 3.7$ –3.9 eV, depending on the crystal orientation and the measurement technique [43].

According to the Drude function, at low frequencies all metals have $\text{Re}[\epsilon(\omega)] < 0$, but as the optical frequency ω increases, $\epsilon(\omega)$ passes through zero at ω_p , to become locally positive. Below ω_p , the $\text{Re}[\epsilon(\omega)] < 0$ condition implies that the collective free electron dynamical response creates a local internal electric field that is out of phase with the external field, and therefore screens it from penetrating into a metal [55,63]. That is why metals make good mirrors [64]. For $\text{Re}[\epsilon(\omega)] > 0$, by contrast, the response phase changes so that the free electron plasma transmits the optical fields as collective plasmon charge density waves causing metals to become nominally transparent [56]. The $\text{Re}[\epsilon(\omega)] = 0$ condition, here referred to as epsilon near zero, or ENZ, is particularly important

to this review, because it defines the bulk plasma frequency, where we find the onset of plasmonic photoemission in silver [41,43,44]. At ENZ the optical field starts to penetrate a metal as a plasmon charge density wave. From nonlinear optical studies it has been shown that the linear response vanishes and nonlinear response nonperturbatively dominates, leading to processes such as high-harmonic generation [65–69]. In a 3D plasma, the optical field cannot directly couple to the longitudinal bulk plasmon mode, but this is possible at a metal/dielectric, *e.g.*, vacuum, interface, where the abrupt onset of the plasma enables a nonlocal dielectric response [55,70–73]. The direct photon-plasmon coupling, in general, is inhibited by momentum conservation because the momentum of a photon, $p=\hbar 2\pi/\lambda=\hbar k$, is much less than that of a plasmon [69,74]. For this reason, plasmons can only be excited when there is an additional source of quasi-momentum, such as a surface, or when the momentum is undefined because of field localization [74,75]. Note that, according to Eq. (3) the transverse plasmon disperses above, but towards, the light line, as can be seen in Fig. 1 of Ref. [55].

The 3D bulk plasmon has the highest frequency response compared with lower dimensional 0-2D responses of metallic plasmas. We note immediately that all of the plasmonic modes are polarization fields. The free electron gas in plasmonic metals is polarized at a resonant frequency by the optical field, and as such polarization field, it can decay by reemitting an optical field into the vacuum. In other words, it is a collective light-matter polariton mode [76]. Light absorption occurs by decay of the polariton mode into single particle excitations, which could be hot electrons, or even more pertinently to this review, photoemitted electrons.

The 0D localized plasmons (LP) are very commonly employed in light energy transduction because they have strong optical resonances. Their resonance properties have been described in numerous publications, and will not be specifically discussed here [8,13,17,20]. It is important to note that their plasmonic properties are malleable by the material choice, size and shape, and their dielectric environment [8,77,78]. Their application to single molecules is of particular interest, because their strong field enhancement enables single molecule detection by Raman, or other polarization sensitive methods [79–83]. LP plasmon modes are said to potentially have their fields localized within single atoms, which has enabled tip-enhanced Raman spectroscopy at the atomic level within single molecules [84]. We emphasize, again, that such spectroscopy employs the plasmon polariton nature. As soon as plasmons decay into hot electrons, they can induce single molecule chemistry, or drive electron currents [20,24,83].

LP modes are sensitive to the plasmonic nanoparticle size, shape, and aspect ratio [78,85]. By stretching a nanoparticle in one direction, one can maintain LP mode response in the short direction, and tune the response in the long direction [86–88]. Such anisotropic particles, thus, have 1D plasmonic responses. Stretching the particle decreases the plasmonic particle resonant energy in relation with its length. One can understand such particles as behaving as 1D plasmonic resonators, where one can image the relationship between their resonator length and plasmonic response by near field microscopy [89], electron energy loss measurements in transmission electron microscope [90–92], or by imaging the nonlinear electron emission in a photoemission electron microscopy [93,94]. Such measurements reveal the energy and space dependent nodal structure of the 1D plasmon modes. One should note that although such 1D structures have bright fundamental responses that tend to a low frequency [92], they also have higher order resonator modes at frequencies that approach the ω_p frequency. Such analysis may not be possible in a simple optical measurements, but becomes evident by spectromicroscopic methods [93,95,96].

Proceeding to 2D, metal/dielectric interfaces support surface plasmon polaritons (**SPPs**). Although this is not the main topic of this review, we note that SPPs have dual character; they are transverse polarization fields that decay evanescently into metal and vacuum for one-half of their cycle, and longitudinal charge density fluctuations during the other-half of their cycle. They propagate at the local speed of light that is defined by the dielectric properties of the interface [97]. For a thin metallic film, the plasmonic modes exist on both of their metal/dielectric interfaces, and support two modes, each having a symmetric or antisymmetric overlap in the center of the film [98]. Although, such modes are interesting in many aspects, we discuss only single interface SPP responses on thick metal samples, primarily forming metal/vacuum interfaces. SPPs exist on smooth metal films that extend over lengths that are comparable, or exceed, $\lambda_{\text{SPP}}/2$ wavelength scales. λ_{SPP} is defined by the dielectric properties of the interface, as $\lambda_{\text{SPP}} = 2\pi/k_{\text{SPP}}$, where $k_{\text{SPP}} = Re[\omega\sqrt{\epsilon_m/(1+\epsilon_m)/c}]$. Here $\epsilon_m(\omega)$ is the dielectric function of the metal with the general Drude form of Eq. (1), which is negative at

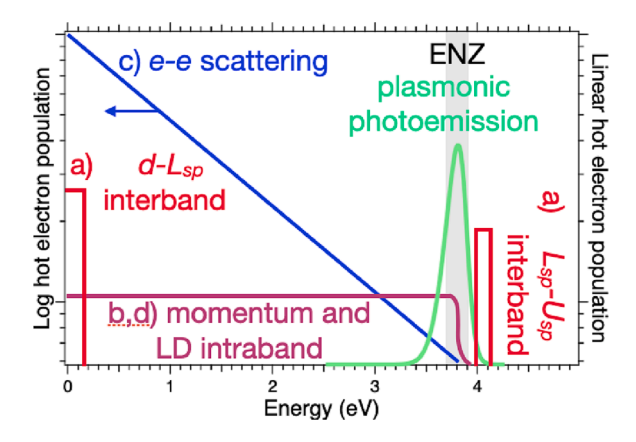


Fig. 1. Energy distributions of hot electrons generated by processes a-d), when exciting Ag in the ENZ region, following the schematic in Ref. 154. In addition, we describe plasmonic photoemission that occurs when exciting Ag at or above the ENZ region. The energy distributions are described qualitatively, but no relative strengths are implied for the different processes.

low frequencies in the intraband region, and causes saturation at $\epsilon_m = -1$, where $k_{SPP} \rightarrow \infty$. SPPs are bound modes that exist only when the sign of Re[$\epsilon(\omega)$] changes across the interface. At low frequencies, the SPP dispersion converges to that of light, and as $\epsilon_m \rightarrow -1$, the SPP frequency saturates at the surface plasmon frequency, ω_{SP} . In the case of Ag, the surface plasmon resonance is $\omega_{SP} \sim 3.68$ eV (there is scatter in the literature values, and a weak crystal orientation dependence [99]).

The field circulation during each cycle of the field oscillation is finding important applications in topological plasmonics [100–108]. While, the spin of optical fields in vacuum is longitudinal, pointing either in the propagation direction of the k vector or against it, the circulation of the evanescent SPPs field in the meridional plane causes their spin to be transverse. This makes SPPs chiral in the sense that changing the sign of their $k_{\rm SPP}$ changes the sign of their spin angular momentum (SAM) [100,109–111]. This property is referred to as the spin-momentum locking [112–114]. Tailoring of the SAM of SPPs by designing methods to generate their orbital angular momentum (OAM), and through spin-orbit interaction of light, to generate plasmonic vortices, is an active topic in topological plasmonics [115–120]. How such spin and vectorial properties of plasmonic fields dress materials in their nearfield is a subject of Poincaré engineering of light-matter interactions [106].

We note at this point that for a free electron metal, the expected surface plasmon frequency is related to the bulk plasmon frequency as $\omega_{SP} = \omega_p/\sqrt{2}$ [6,55]. This is not the case with Ag, where ω_{SP} is <0.2 eV below ω_p [121]. This is a consequence of the occupied d-electron bands participating in the non-local screening in Ag [73,122,123].

Exciting and imaging SPP modes of plasmonic metals has been an active topic of research [75,103,107,108,124–131], and provides a route to tailoring their spatial and temporal properties. Because the SPP dispersion function is below the light line, one must supply momentum to couple the optical and SPP fields [69]. This has been done traditionally by the Kretschmann geometry [132,133], where the optical field enters from the high index of refraction dielectric material into a metal film such that the light and SPP dispersions intersect. This may work under some circumstances, but it is not ideal for the nanoscale tailoring of the space–time properties of SPP fields. A different route is to generate a coupling structure, where the metal film is cut or structured, usually by lithographic methods, on a subwavelength scale [108,124,134–136]. An optical field polarized perpendicular to such a film discontinuity (metastructure) can excite an LP response, and because the LP response momentum is undefined, it will decay into the SPP mode of a metal field in its near field region [137]. This coupling mechanism is remarkably efficient, so that it is possible to monitor the SPP propagation by interfering it with a phase correlated optical probe pulse [75]. This is the basis for interferometric time-resolved photoemission electron microscopy (ITR-PEEM) imaging of SPP dynamics on the nanofemto scale [75,108,124,135,136,138–140].

The lithographic design of SPP coupling metastructures can define various functions, such as the SPP focusing in space and time, the OAM carried by an SPP field, the SPP standing and propagating waves in resonators, *etc* [125–127,134,140–142]. The design of OAM is particularly interesting in topological plasmonics, because it defines the spin–orbit coupling of propagating SPP fields [103,107,108,129,143]. It is also significant that optical spin affects the SPP coupling. For example, the projection of the optical spin of the exciting light onto the SPP spin defines the strength of their coupling [134,137,144]. This is the basis for the plasmonic spin-Hall effect where the SPP focusing location by a plasmonic lens depends on the spin of the optical field [137]. The plasmonic spin-Hall effect is similar to the quantum spin Hall effect of electrons, and it provides a method to focus spin of different sign in specific locations [134].

The surface SPP mode is a monopole response, which is another reason why it cannot be excited directly by optical fields [55,145]. Below the bulk plasmon frequency resonance, metals also have the multipole plasmon response [123,145,146], which generates electric fields with the opposite sign to an incoming optical field, and thus screens its penetration into a metal [63]. This multipole response is dominantly dipolar in nature so that it can be effectively excited by light, but unlike SPP mode, it does not propagate; it defines the local field strength at a metal/vacuum interface, which deviates from the classical Fresnel response of a metal [54,123,147,148]. The centroid of this screening charge density is defined by the Feibelman's $d_{\perp}(\omega)$ parameter [71], which quantifies deviations from the Fresnel response [72]. The maximum of the multipole response, ω_m , is typically at $\omega_m = 0.8\omega_p$ [63,145], but above ω_{SP} . Because for silver ω_{SP} is just below ω_p , the ω_m is squeezed in between them [50,149]. The multipole plasmon can be considered the surface counterpart of the bulk plasmon that responds at a lower frequency, because electrons penetrating into the vacuum have a lower electron density than the bulk metal [150–152]. To end the introduction to plasmonic modes, the theoretical study by Gumhalter and Novko considers the Floquet engineering of plasmonic photoemission in the nearfield of SPP waves in silver, where such lightmatter wave can excite nonlinear responses in its nearfield [52].

2. Hot electron generation

Before proceeding to describe plasmonic photoemission, which describes a route of how plasmonic fields decay into single particle excitations, we first introduce a related topic of what we consider to be the community consensus on how plasmons decay into hot electrons. Although, we mainly wish to refine and add to this consensus, we assert that it is largely untested by experiment and incomplete. For this purpose, we describe different processes for hot electron generation based on concepts that are frequently invoked in the literature, though they are rarely tested or understood. We follow the detailed reasoning for the generation of different hot electron distributions based on Refs. [153,154]. While there are many statements in the literature of what the putative distributions could be, these publications rarely give specific justifications for them [153,154]. Similar theoretical descriptions of plasmonic hot electron generation can be found in other research as well [155].

Fig. 3 of Ref. [154], introduces four different mechanisms for electron-hole (*e-h*) pair generation in metals that produce characteristic distributions given in Fig. 4 of the same, and are here schematically reproduced in Fig. 1. The thesis for hot electron generation is that optical fields and plasmons interact with metals by polarizing a free electron gas, and therefore have similar outcomes in the *e-h* pair generation [156]. We adopt this view, for the most part, but emphasize that the publication by Gumhalter and Novko has a

rigorous presentation of light-matter interaction, particularly under nonlinear conditions [52]. The mechanisms described in Ref. [154] can be summarized as 1) interband excitation; 2) momentum scattering intraband transitions; 3) *e-e* umklapp scattering transitions; and 4) Landau damping. We will briefly describe these processes and address to what extent they can and do appear in experiments that probe electron dynamics in metals. Our interpretation of single particle excitations in metals is based on TR- and AR-mPP spectroscopy, which typically probes the coherent polarization and population dynamics in metals with < 20 fs time resolution [39,40,157–162]. Moreover, with 10–20 fs time resolution, it is the closest that the primary hot electron distributions are characterized in the literature. Simply, in a nonlinear excitation one (or more) photons generate a primary excitation in a metal; and the subsequent one (or more) photon absorption emits such electrons into the vacuum, where their energy and momentum distribution are recorded, and consequently related to the primary intermediate state distribution [2,36,163]. We do not refer to all optical spectroscopic studies relating to hot electrons, because they interrogate energy and momentum integrated information, though, if properly interpreted, this can be useful [164–170]. Furthermore, we add the plasmonic photoemission distributions that we have observed for ENZ excitation, and will be described in the upcoming Section V. In the following we will refer to the single particle and plasmonic excitations, as appropriate.

- **a. Interband excitation.** Depending on the laser excitation photon energy, interband excitations give rise to bright spectroscopic features in *m*PP spectra involving nonplasmonic mode excitations [3,39,159,161,162,171]. Plasmonic responses are generally strongly damped when they overlap with interband transitions. Nevertheless, plasmon decay to generate interband *d* to *sp*-band *e-h* excitation has been reported in activating chemical processes [172]. Interband processes in *m*PP spectra are useful to calibrate other signal components that can be attributed to intraband plasmon decay processes [41,43,45], as will be shown. Although bulk bands have 3D dispersions, interband transitions, as detected by *m*PP spectroscopy are well localized in the available energy—momentum space by the energy and momentum conservation requirements, as well as how they define the optical transition dipole moments. The remaining plasmon decay processes to be described involve intraband scattering.
- **b. Momentum scattering intraband transition.** Intraband absorption is a well-known process that dominates light absorption below the interband absorption onset in metals [173,174]. Although photons cannot induce momentum conserving transitions in free electron bands, this can happen through a second-order process involving either phonon or defect scattering [175–177]. In spectroscopy of metals, this is broadly referred to as the Drude absorption [174,178–180]. Because the phonon energy is usually small compared to that of a photon, nearly all the photon energy can be transferred to excitation of *e-h* pairs [37,154]. Defects modify the potentials experienced by electrons on the screening length scales. Such local potential discontinuities are sources of momentum without taking up the plasmon energy. These second-order scattering processes can be minimized by lowering the sample temperature to minimize the phonon absorption [181], and by regulating the sample crystallinity and purity.
- c. Umklapp e-e scattering. Optical fields can induce intraband acceleration electrons within the conduction band of a metal. Electrons thus gain kinetic energy within a fraction of an optical cycle, but, unless there is a source of momentum, light cannot be absorbed. Although field induced intraband currents are of great current interest for high harmonic generation and Peta Hertz optoelectronics [182–186], we are not interested here in high field phenomena here. Instead, light can be absorbed by an e-e scattering process where an electron promoted to a virtual state scatters with an electron in the Fermi sea, and total momentum is conserved by either normal or Umklapp scattering process, where additional momentum is gained by scattering with the lattice vectors [36,154,187]. While it is possible that such processes promote intraband absorption, it is not particularly desirable because the photon energy is immediately divided among two e-h pairs, that is, four quasiparticles. The predicted hot electron distributions from such processes peak at low energies, which in 2PP spectroscopy, would appear at the vacuum level, and the probability diminishes towards energy of $E_F + \hbar \omega$. Though such processes are not favorable for transferring the plasmon or photon energy to hot electrons, there is strong evidence that the predicted energy distributions are actually observed in mPP spectra [43,188]. One should note that conventional (linear) photoemission spectra, in addition to expected features from the occupied bands, have a broad distribution that peaks at the vacuum level. This is usually inelastic signal named the Shirley background [189,190], which refers to the contribution from electrons that are excited above the vacuum level, but undergo inelastic scattering before emerging into the vacuum. The inelastic scattering can involve scattering with defects, phonons, or e-e scattering. Such processes are not confined to plasmonic excitations, but have been understood as the inelastic product that accompanies the elastic spectra, particularly in the core-level photoemission
- **d. Landau damping.** Landau damping is the most difficult concept to explain both for experimentalists and theorists. The theory described by Landau concerns the decay of collective plasmon modes of infinite 3D free electron plasmas, without a reference to edges or mode of confinement. The exchange in energy between single particles and collective modes relates to the relative single particle velocity compared to that of the collective wave. Single particles are said to surf on the plasma wave, and as such can gain or lose energy from the collective mode [191–194]. This is expressed in Fig. 3 of Ref. [55], which shows the weakly dispersing longitudinal plasmon mode intersecting with the strongly dispersing single particle continuum, which enables momentum conserving transitions between them. This description is oversimplified, because the plasmon dispersion meets the single-particle dispersion in all orders of perturbation theory [195]. Landau damping becomes particularly strong in nanostructured metals, and near metal surfaces because of the folding of intraband transitions such that there are multiple crossings with the longitudinal plasmon mode. This can be understood as enhanced electron scattering due to size dependent quantum confinement [196,197]. Quantum confinement indeed enables optical transitions to occur in thin Ag films and nanoparticles, that have been detected by *mPP* spectroscopy [135,198]. Expanding on the definition of Landau damping, the momentum scattering intraband transitions can be included in this process, where the source of momentum that couples the collective and single particle excitations are phonons or defects.

3. Hot electron energy distributions

So far, we have discussed in II.c the secondary hot electron distribution that results from e-e scattering processes and decays towards the high energy limit of spectra; in mPP spectroscopy experiment such distribution would generate the maximum hot electron population at the low energy limit work function, E_V, edge, that tend to approximately decay in intensity with an exponential profile towards the E_F edge. The hot electron energy distributions from II.b and II.d processes are presumed to be more effective for harnessing plasmon energy in form of hot electrons that they generate [153,154]. These hot electron distributions are alleged to depend on the joint density of hole and electron states that define the e-h pair energy that is generated. For a free electron band, they are described as generating a flat distribution in in energy for generation of hot electrons in E_F to $E_F + \hbar \omega_L$ range and for holes in the E_F to $E_F - \hbar \omega_L$ range, where $\hbar\omega_L$ is the excitation energy. For simplicity, we will call this the "rectangle" hot electron distribution, which is the default that can be found sketched in numerous publications, reviews, and theoretical calculations [154,199–201], and is sketched in Fig. 1. We argue, however, that such distributions have never been supported by experimental data that can directly record the primary hot electrons, but are used to explain the chemical products and excitations attributed to them. While such distributions may be reasonable for processes in II.b and II.d, we argue that there is growing evidence that the decay of plasmonic modes leads to preferred excitation of electrons from E_F , resulting in plasmonic photoemission. Moreover, rectangular distributions are inconsistent with the electronic band structures of metals, beyond those that fit the free electron model over a broad spectral range. Presumably, the existence of plasmonic modes does not void the electronic band structure of the supporting material, and its role must somehow be reflected in hot electron distributions.

In a 2PP experiment one can measure coherent and incoherent two-photon excitation processes. In such experiment electrons excited by the pump pulse are probed by excitation with a second photon to above the vacuum level, to be photoemitted and measured with respect to energy and momentum. While coherence in one-color experiments is interesting for understanding the creation and decay of polarization fields [39,157–159], two-color experiments measure populations [202], and thus, provide less information and invite less interpretation.

Perhaps the first experiment that sparked interest in hot electron studies by 2PP method was that of Fann et al. on polycrystalline gold. This experiment used a visible pump pulse to generate hot electrons, and a UV probe excitation to induce photoemission. Their experiment had ~ 200 fs time resolution, which is insufficient to compete with e-e scattering [28]. This is confirmed by their 2PP spectra, which, when plotted on a log intensity scale show a weak signal from $E_F + \hbar\omega_L$ potentially suggestive if a rectangular hot electron distribution ever existed, it had substantially relaxed within the experimental time resolution. Based on other measurements [38], however, one can expect that the lifetime of hot electrons at $E_F + \hbar\omega_L$ in Fann et al. experiment was on the order of 30 fs, and thus their experiment is broadly insensitive to the primary hot electron distribution [28]. Rather, the experiment measured a hot electron distribution that could have undergone several cycles of e-e scattering. Therefore, it is not surprising that the hot electron distributions peaks at the vacuum level edge of spectra where low energy, partially relaxed hot electrons should appear. In another experiment, Lehman et al. performed 2PP experiments on Ag nanoclusters on graphite with 43 fs time resolution. They excited the LP mode of Ag nanoclusters with $\hbar\omega_L = 3.1$ eV light [203]. Like the Au experiments, their hot electron distributions peak at E_V and decline exponentially towards the $E_F + 2\hbar\omega_L$ edge. Their conclusion was that single photoelectrons are dominantly generated by a simultaneous two-plasmon decay, so that their photoelectron distribution did not reflect that of the intermediate state the hot electron population

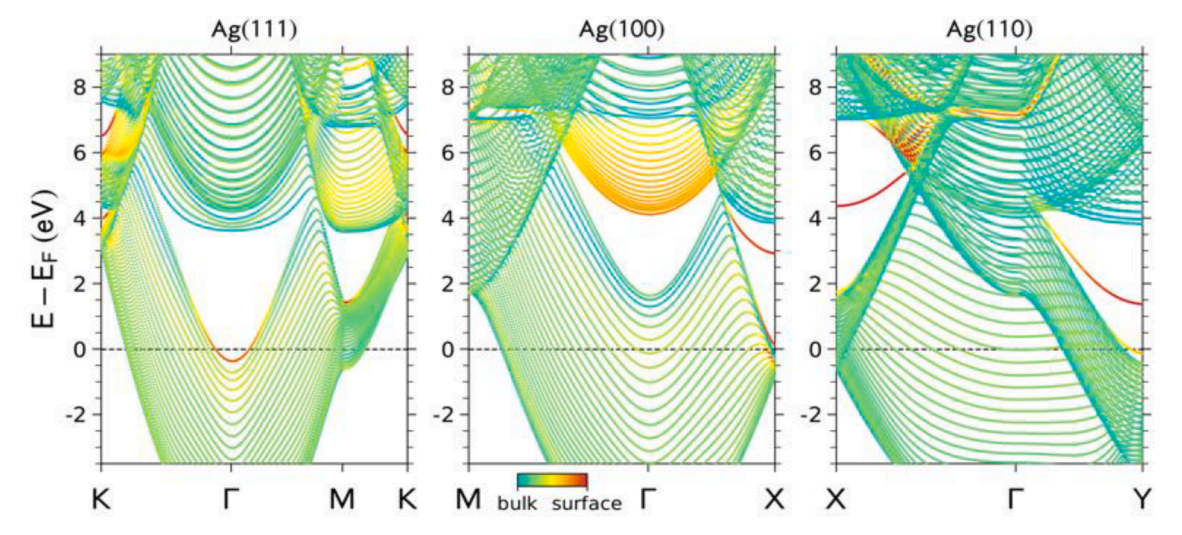


Fig. 2. The electronic bands of silver projected onto the Ag(111), (100), and (110) surfaces from a DFT + U calculation, with PBE functional. The color scale conveys the relative surface vs. bulk wavefunction localization. Surface states are generally depicted in red, unless they are near a band gap edge, which gives them bulk penetration. The quasi-parallel bands are sections of bulk bands for different k_{\perp} . L_{sp} and U_{sp} designate the lower and upper sp-bands. We thank Dino Novko for calculating these electronic band structures. (For interpretation of the references to color in this figure legend, the reader is referred to the web version of this article.)

[203]. Later, 3PP experiments by Tan et al. on Ag nanoclusters on graphite with $\hbar\omega_L = 2$ eV, ~ 20 fs pulse excitation, which does not couple strongly to the plasmon mode of the clusters, found: 1) evidence for coherent charge transfer from Ag-graphite interface state to the graphite interlayer band; and 2) hot electron signal whose energy distribution declines exponentially from the E_V edge and which shows no sign of the $E_F + 3\hbar\omega_L$ edge [27]. This experiment is the only direct observation of coherent, photoinduced charge transfer from a metal nanoparticle to the conduction band of the substrate [27]. Such direct excitation has been predicted [204], and is often invoked in photocatalytic and photovoltaic processes [205], without any direct evidence [8,9,13,20]. The exponentially declining hot electron distribution found for hot electrons in this system is consistent with the exceedingly fast hot electron thermalization in graphite [188,206,207].

We do not wish to discuss details of e-e scattering in this review, however, because the physics has been largely understood for>60 years [208], and reliable experimental results are reported in the literature [2,38]. Let us just state that hot electron lifetimes due to e-e scattering decrease with E² dependence, where E is the energy above the Fermi level. This energy dependence is based on the free electron scattering density of states [208,209], but in real, particularly anisotropic, materials deviations may occur [210]. Interested reader should consult the extensive experimental and theoretical literature on the matter [2,38,209]. We emphasize, however, that the evidence for the rectangular distribution from 2PP spectra would be a distinct appearance of a Fermi edge resulting from photoemission of the primary hot electrons by a probe pulse. Such spectra are not observed, because experiments either lack the sufficient time resolution to probe the electron lifetimes of the primary hot electron distribution, or else, such distributions are generally not produced.

4. Where are hot electrons in the momentum space?

Our goal is to introduce the plasmonic photoemission, which captures a significant plasmon decay process into hot electrons that has a solid experimental and theoretical basis, but is not discussed in the prevailing literature; we rediscovered plasmonic 2PP in Ag single crystal surfaces [41,43,45]. Before we get into the main topic of this review, however, we discuss what is known about hot electron generation in Ag based on 2PP experiments on single crystal surfaces in one- and two-color experiments. The following discussion will require a basic understanding of the band structure of Ag. For this purpose, in Fig. 2 we present the theoretical band structure of Ag for the low index (111), (100) and (110) surfaces, for which we will discuss the possible hot electron momentum distributions and evaluate 2PP spectra for interband and intraband hot electron generation in the ENZ region. Although the bands structures of Ag have been presented many times in the literature at different levels of theory, our calculations are novel in that they strive to evaluate the surface vs. bulk localization of the electronic bands. The calculations are performed for 51 atomic layer slabs for the three low index surfaces. The quasi-parallel lines depict bulk bands with different k_{\perp} in the Γ -L (111), Γ -X (100), and Γ -K (110)

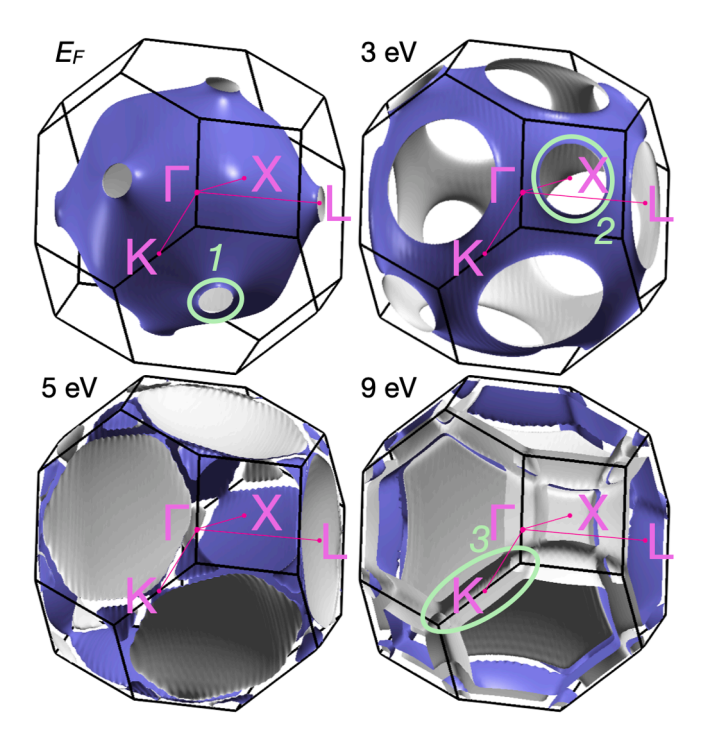


Fig. 3. Isoenergy electronic band surfaces of Ag that define the regions where hot electrons can exist starting, from the Fermi level, E_F , and a 3, 5, and 9 eV above E_F . Blue and gray designate convex and concave surfaces. Γ-L, Γ-X, and Γ-K indicate the [111], [100], and [110] crystal axes, and the ellipses "1–3" locate their projected band gaps. We thank Dino Novko for calculating these surfaces. (For interpretation of the references to color in this figure legend, the reader is referred to the web version of this article.)

direction from a DFT + U (U = 3.1 eV) calculation. The (111) and (100) surfaces have well-known band gaps that reach widths of several eV, as will be related to momentum dependent hot electron distributions shortly. The (110) surface has a minigap at ~ 7.2 eV that supports a surface state, which plays an important role in plasmonic photoemission. The color gradient shows the relative surface vs, bulk character of each band, with strongly surface localized bands appearing mainly in red.

Note that the band structures of all three surfaces show image potential (**IP**) states, which are not accurately calculated by DFT, because it does not describe the long-range image Coulomb potential [211]. Because this is not the main topic of this review, the properties of IP states are well known, and calculations involving many-body perturbation theory that can provide accurate energies are prohibitively time consuming and expensive [212], no attempt is made to perform accurate calculation of the IP states. The unexpected IP states, without inclusion of the long-range Coulomb potential appear at 4 eV and above, most prominently in the band gap of Ag(100) surface. They appear prominently for their yellow surface contrast in the 4–7 eV range. Above 7 eV they become surface resonances and attain green contrast. It may be surprising to find IP states above the vacuum level, but such states exist and have been detected in *m*PP experiments on Cu(100) [171]. These are bound states in the continuum [213], or colloquially referred to as electrons in limbo, because their kinetic energy is locked in surface parallel motion; to decay into the vacuum or bulk metal, they must gain perpendicular momentum and kinetic energy. The band structures were calculated by Novko, in a similar manner as in Ref. [45]. We thank Novko for discussion of the calculated band structures and their notable features.

The mechanisms for hot electron generation by processes described in section II.a-d should be operative both in single or polycrystalline materials. Single crystalline surfaces strictly define the phase space for hot electron generation and thereby enable discussion based on the intrinsic atomic scale material properties, their generally understood light-matter interactions, and their characterization by mPP methods. Polycrystalline surfaces open additional momentum scattering channels that can facilitate hot electron generation by generalized Landau damping. We start by presenting the isoenergy surfaces of electronic bands of Ag in Fig. 3, which define, and more precisely, restrict the phase space for hot electron generation. The electronic band structure in Fig. 2 shows that all three surfaces have band gaps that must be considered in the energy–momentum distribution of hot electrons that can be generated in single crystal surfaces. In polycrystalline films the same concepts hold for hot electron generation, though the presence of band gaps may not be easily discerned. The surfaces in Fig. 3 are shown for the Fermi level, and $E_F + 3.0$, 5.0, and 9.0 eV energies, based on standard electronic structure calculations such as in Fig. 2 [44].

The electronic *iso*-energy surface of Ag has a nearly spherical shape that defines momentum regions where the free electron *sp*-band crosses the Fermi level and bulk electronic bands exist. A nearly spherical Fermi surface is expected for a free electron metal, but in the case of noble metals, at the Fermi level, there are projected band gap openings in the Γ-L (111) directions indicated by "1" in Fig. 3 [175,214]. This band gap spans -0.4 to 3.9 eV energy range [215]. The surface at 3.0 eV energy shows the Γ-L gap growing larger in the *k*-space and another band gap indicated by "2" opening in the Γ-X (100) direction. This gap spans the 2.0–6.6 eV range [215]. The two band gaps substantially confine the phase space for hot electron generation. In other words, hot electron population is excluded from the energy–momentum space within the band gaps where eigenstates do not exist. By contrast, in the Γ-K (110) direction there is no band gap between E_F and E_V , that would restrict hot electron generation. We discovered, however, a Γ-K minigap indicated by "3", which is predicted by theory at 7.0–7.3 eV, in conjunction with plasmonic photoemission. Experimental 2PP spectra of Ag(110) surface, show that this gap actually exists at a slightly higher energy, as will be described [45].

The band gaps restrict the phase space for hot electron generation from plasmon decay, as we will explain with respect to the band structure for specific crystalline directions. Surprisingly, much of the plasmonics literature, experiment and theory, treats noble metals within a free electron model that fails to restrict to the phase space for hot electron generation according to their well-known band structures. For example, the calculations by Goddard, Atwater and coworkers [199–201], describe the 4D energy and momentum dependent intraband and interband electron and hole excitation in noble metals. Their calculations describe the role of the band gaps in restricting the phase space for hot electron excitation and energy and momentum dependent lifetimes. Unfortunately, their momentum averaged pictures of electron distributions, which are often reproduced in the literature, convey misleading impression that intraband hot electrons are generated isotropically to form rectangular distributions. The calculations by Lischner and coworkers [17,216] are also distinct in that they reproduce the known band gap-restricted hot electron distributions in noble metals. The experimentally measured electronic excitations with emphasis on the momentum dependent intraband hot electron distributions are described in more detail, next.

a. Ag(111). We consider first the 2PP spectra of Ag(111) when excited by $\hbar\omega_L = 3.1$ eV femtosecond light pulses based on the analysis of Pontius et al. [190,217]. At this excitation energy, two-photon photoemission can occur through two-photon absorption through real or virtual intermediate states. The excitation is far from ENZ, so we do not expect a strong plasmonic contribution. As noted above, the band gap of Ag(111) does not support bulk bands in the Γ-L direction. The only states that exist within the band gap are the partially occupied Shockley surface state (SS) with a band minimum of \sim -0.06 eV below E_F and the unoccupied n=1 image potential (IP1) state at \sim 0.75 eV below E_V [218–220]. These two states will be observed in mPP spectra of any order no matter what is the resonance condition, as we have experienced so far [39–41]. The SS exist due to the termination of Ag crystal, while IP states result from electrons having an attractive Coulomb interaction with their screening image charge [221,222]; they form a Rydberg-like series that converges to E_V [223], where the IP1 state generally has the highest transition moment among the IP state series in 2PP spectra because it has the largest density at the surface. The IP states are not correctly predicted in the band structures of Fig. 2, because DFT does not describe the long-range image potential, which develops in response of excitation of electrons in front of a metal or dielectric surface [221,222]. Lacking real intermediate bulk states, the momentum conserving transitions at the Γ-point must occur through virtual states.

We have simulated *2PP* spectra with 3.1 eV excitation based on a model that was developed for conventional, single photon, UV excited photoemission from Ag(111), leading to photoemission with approximately the same final energy states [224]. The simulated

spectrum in Fig. 4, can nearly entirely be attributed to coherent 2PP process starting from the lower sp-band (L_{sp}) above E_V , from where electrons emerge into the vacuum [190]. The U_{sp} acts both as the dominant nonresonant intermediate state and the real final state for the nonlinear two-photon transition. There are components in the 2PP signal that have no band structure origin: one is a phonon induced component that depends on the sample temperature, and can involve electron scattering into the normal emission (k_{\parallel} =0 Å⁻¹) direction at the initial, intermediate, or the final state stage; while the other [190] is the Shirley background [189] representing final state electrons that scatter prior to emerging into vacuum in the normal emission direction. These photoelectrons that are excited by a second-order process do not carry spectroscopic information, but their energy dependence can modeled as an integral over the directly excited states at higher energies [189]. These 2PP spectra show vanishingly small evidence of hot electron generation in the intermediate states, as they cannot be generated as real states within the projected band gap by some inelastic scattering process [190]. Electron–phonon interaction enables electrons excited above the vacuum level into bulk bands to scatter into the surface normal direction to be photoemitted. In this process, however, they lose their band structure signature on account of momentum scattering. Temperature dependent 2PP spectra confirm the contribution of electron scattering into the surface normal direction, where this secondary contribution to 2PP is detected. This scenario for the nonlinear 2PP at Ag(111) surface is further confirmed by investigating the off-normal photoemission [217].

b. Ag(100). Next, we consider the possibility of hot electron generation in the (100) crystalline direction. For this we examine one-color ($\hbar\omega_L=4.60$ –4.95 eV) 2PP spectra from Ag(100) surface (Fig. 5). These spectra were recorded at Marburg University in the Höfer group by Marks [225]. The spectra show dominant features due to the IP1 and IP2 state excitation, a weak feature due to the U_{sp} excitation, and two-photon excitation from an occupied Tamm surface (TS) state near the top of the d-bands. By plotting the final state energy E_{fin} vs. the photon $\hbar\omega_L$ energy in Fig. 5(right), one can determine from the slope the number of photons that excite photoemission from a population in the initial $(2\hbar\omega_L)$, or intermediate $(1\hbar\omega_L)$ states that participate in the 2PP process. Moreover, the plot intercepts give the energy of the source state for the photoemission process. Thus, the intercepts define the bulk free electron band, U_{sp} as the final state (indicated as sp-band), IPn as the intermediate states, and a Tamm surface state (TS) as one of the initial states. Such plots help to assign the sharp peaks that appear in $\hbar\omega_L$ dependent 2PP spectra. If one finds a $0\hbar\omega_L$ slope, however, it could signify that the excitation occurs to a final state in the photoemission continuum, or else, is a signature of non-Einsteinian process where the excitation light excites a fixed internal field (think bulk plasmon), and this field excites photoemission from a narrow range of initial states (e.g., from the Fermi level) [41,43].

Based on these spectra, one might ask where is the hot electron population? There is no rectangular distribution, that one might expect from hot electrons. Instead, there is a broad distribution from E_F to $E_F + 2.0$ eV that has some vague structure. Marks finds that hot electrons populate the L_{sp} states that exist at $k_{\parallel} = 0$ Å $^{-1}$ up to $E_F + 2.0$ eV, where the projected band gap in the [1 00] direction opens up [225]. These states must be populated by intraband absorption, because mainly the L_{sp} can act as the initial source state of electrons in this energy region. Nevertheless, there also appears to be an interband contribution from excitation from TS to the L_{sp} . Though this can be a first order process, it is not substantially stronger than the intraband absorption from the L_{sp} . The hot electron population **does**

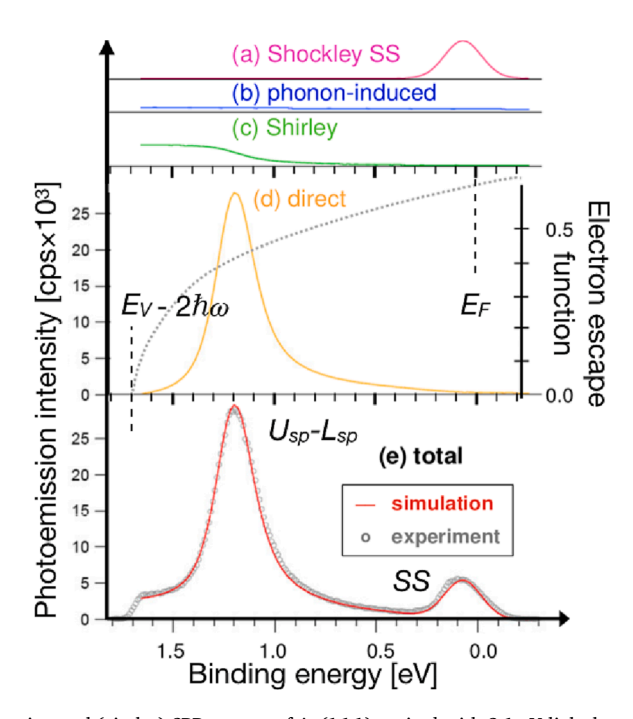


Fig. 4. a-d) Simulation of e) the experimental (circles) 2PP spectra of Ag(111) excited with 3.1 eV light based on the dispersion of the L_{sp} and U_{sp} bands [190]. The components are separated into direct bulk and SS two-photon absorption, Shirley final state scattering, and phonon induced component that includes hot electron processes. The dotted line shows the energy dependent electron escape function.

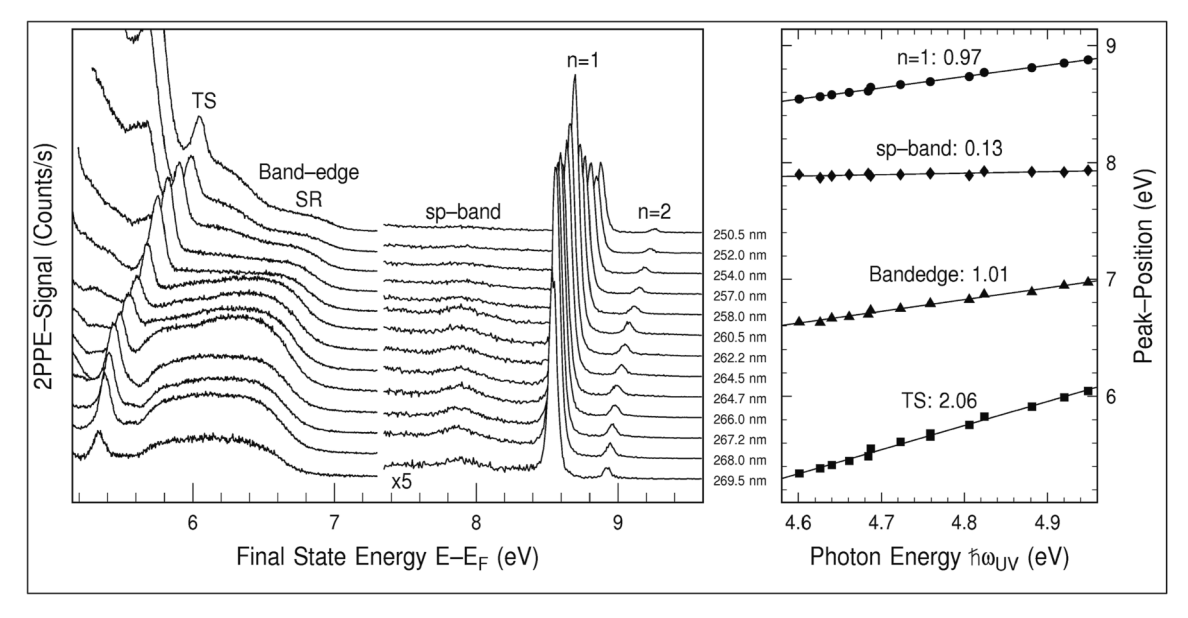


Fig. 5. (left) 2PP spectra of Ag(100) with UV excitation below and above E_V showing IP1 and IP2 states, the U_{sp} band, and the hot electron region that extends to ~ 2 eV above E_F . Below 2 eV there is a surface resonance, which contributes to the band edge signal where the [100] gap opens. TS indicates an occupied Tamm state. (right) The tuning of photoemission energies of different features with $\hbar\omega_L$. The slopes of ~ 0 , 1, and 2 define the features as the final, intermediate and initial state in 2PP process. As $2\hbar\omega_L$ is increased, one photoemission signal starts to dominate the signal at low final state energies. We thank Manuel Marks and Ulrich Höfer for providing the figure [225].

not extend up to $E_F + \hbar \omega_L$, as one might expect from the free electron model, because there are no states available for them above 2.0 eV in the [100] direction. The spectra in Fig. 5 show beautifully that the band structure matters to hot electron generation. We note, however, that the distribution between $E_F + 2.0$ eV is not very flat, most likely because in that region there is an unoccupied surface resonance at ~ 1.3 above E_F , which has the same origin as the Shockley Surface states of Ag(111), but by coinciding with the bulk bands into which it can propagate, it becomes much broader [43,226].

c. Ag(110). So where are the hot electrons? They can be found when examining the 2PP spectra of the Ag(110) surface, which does not have a projected band gap in the [110] direction below E_V near the surface Brillouin zone center (Fig. 6). Therefore, incoherent 2PP occurs where the pump pulse excites intraband hot electrons within $L_{\rm sp}$, and the probe pulse induces their photoemission [43,45]. Note that the spectra in Fig. 6 are excited at approximately the bulk plasmon frequency, $\omega_{\rm p}$. When $\omega_{\rm L} < \omega_{\rm p}$, the hot electron signal is still seen, so both the direct and plasmon mediated excitation generates hot electrons [45].

The (110) surface is anisotropic with close packed lines of Ag atoms propagating in the [001] direction and two atom wide ridges

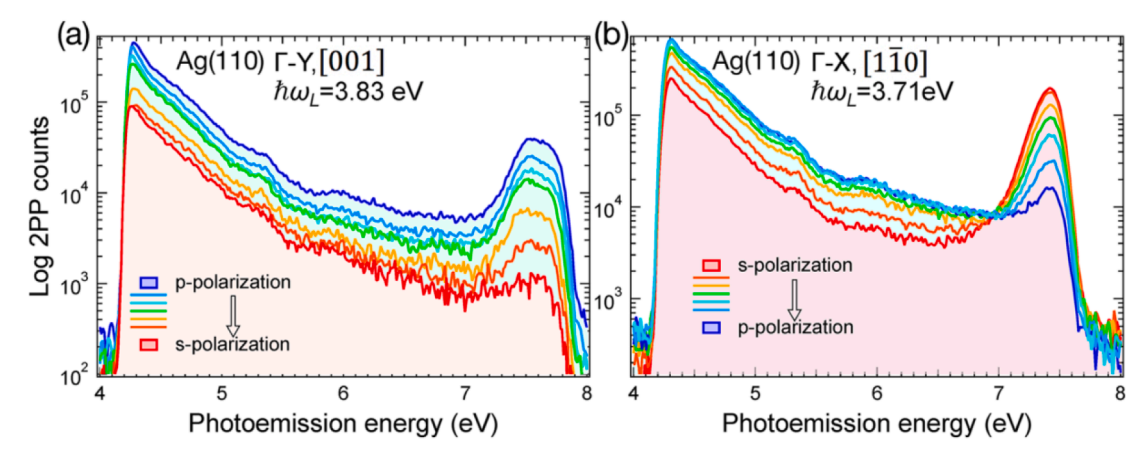


Fig. 6. Photoemission spectra of Ag(110) surface, that does not have a bandgap below $\hbar\omega_p$. The spectra have two components: hot electron population decreases from E_V with nearly exponential dependence towards $E_F + 2\hbar\omega_L$ edge, where the plasmonic photoemission, $2\hbar\omega_p$, feature appears. a) 2PP spectra when the sample Γ-Y or [001] direction is in the optical plane and p-polarized light has a surface parallel component in the corrugated [001] direction. b) Same for the sample oriented in the Γ-X or [1 $\bar{1}$ 0] direction where s-polarized light points against the [001] corrugated direction. Note the logarithmic vertical scale. Reproduced with permission from Ref. 43.

and troughs from conjunctions of proximate (111) surfaces modulating the surface height in the [001] direction (see Fig. 7c). The 2PP spectra in Fig. 6; are measured as a function of the laser polarization; p-polarized light incident on the surface with 45 angle with respect to the surface normal has a field component that is normal to the surface, and s-polarized light is either parallel or perpendicular to the surface corrugation in the [001] direction depending on the crystal orientation. The polarization dependence of these spectra are unexpected, and will be addressed later [43]. The spectra have maxima at the low energy E_V edge, and decay approximately exponentially towards high energy corresponding to $E_F + 2\hbar\omega_L$ signal. The peaked signal at the $E_F + 2\hbar\omega_L$ limit is the plasmonic photoemission signal to be discussed in conjunction with that of the other surfaces [43].

It can be concluded from the spectra in Fig. 6 that they are dominated by incoherent processes involving hot electron photoemission because sharp spectroscopic structures characteristic of interband transitions are not expected to occur for $\hbar\omega_L$ of the measurement. Because the distribution departs significantly from rectangular, one might anticipate that it could be significantly relaxed by *e-e* scattering, as anticipated in Ref. [154]. Whether this occurs during excitation by the II.c process, or is a consequence of relaxation of the primary population, is unclear. While the excitation pulse duration is ~ 30 fs, the *e-e* scattering lifetimes of 3 eV hot electrons in Ag are predicted to be < 10 fs [38]. Thus, hot electrons could have undergone relaxation during the 2PP excitation, and therefore the observed spectra may not be representative of the primary hot electron distribution. This is a nice example that capturing the rectangular electron distribution, if it is ever generated, may be extremely difficult. A corollary is that harvesting energy of the primary hot electrons at chemically relevant energies may be extremely challenging.

We emphasize that in considering 2PP spectra of Ag(110), one cannot solely rely on the k_{\parallel} =0 Å⁻¹ data, such as in Fig. 6, which lack single particle spectroscopic structures and are dominated by the hot electron signal and the plasmonic photoemission. This signal does not represent the total optical response of the Ag(110) surface, and might give the impression that light absorption is dominated by intraband processes. Therefore, it is important to examine 2PP spectra of the Ag(110) surface over a broader k_{\parallel} range. Because the (110) surface forms at a conjunction of two (111) surfaces, one might expect that the interband transitions that play a dominant role for (111) surface, also occur at the (110) surface, but appear in an off-normal direction [42]. This is in fact the case [45,227,228]. Fig. 7 shows 3D energy-parallel momentum 2PP spectra of Ag(110) that is taken in a momentum microscope photoemission apparatus in the Mathias Group at the University of Göttingen [45,229,230]. One sees that when recording photoemission in the [001] direction, a plethora of sharp dispersive bulk and surface interband transitions appear, in addition to the hot electron signal with a maximum at the E_V limit, as well as the strongly anisotropic plasmonic signal at the E_F + $2\hbar\omega_L$ limit. We emphasize this complexity because when someone discusses a rectangular hot electron distribution, it is likely that they have not considered optical excitation in metals at any

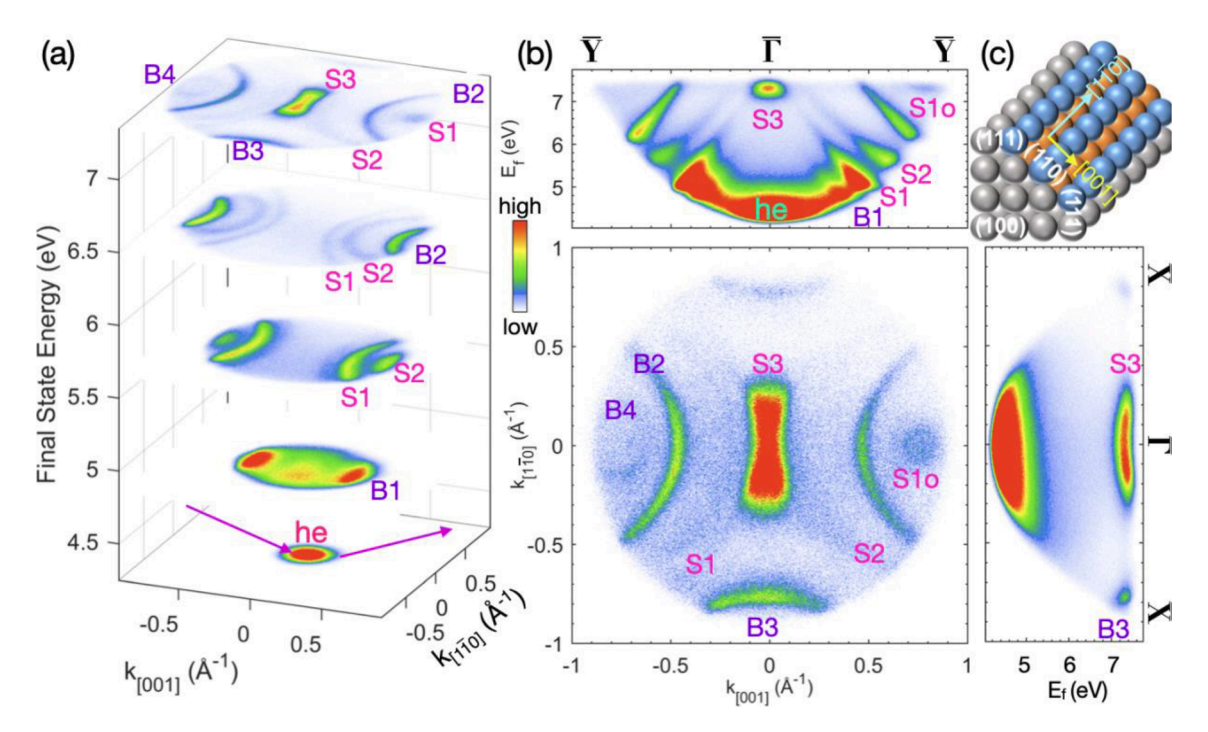


Fig. 7. Momentum microscope 3D energy-parallel momentum (E_{fin} , $k_{||\Gamma Y}$, $k_{||\Gamma X}$) 2PP spectra of Ag(110) with $\hbar\omega_L=3.72$ eV p-polarized excitation and the sample with the corrugated Γ-Y or [001] direction in the optical plane. a) E_{fin} cross sections through the 3D spectroscopic data. b) Cross sections through the data in a) along the Γ-Y direction (top), Γ-X direction (right) and through $E_{fin}=7.4$ eV. The features labeled with "B" and "S" refer to the bulk and surface interband transitions; specific assignments are reported in Ref. 45. S3 is the $2\hbar\omega_p$ feature, which is exceedingly anisotropic. Regions where hot electrons appear are indicated by "he". c) The atomic structure of Ag(110) at the junction of two (111) surfaces (The (111), (100), and (110) planes are indicated). The blue and orange balls indicate the top and bottom Ag atoms of the two-atom wide corrugation in the [001] direction. Ag atoms in the [110] direction are close packed. Adopted from Ref. 45. (For interpretation of the references to color in this figure legend, the reader is referred to the web version of this article.)

level beyond an idealized free electron gas. Moreover, even if a material has a plasmonic response, this is a polarization field, and light is only absorbed when the collective response excites single particle e-h excitations. The bulk band structure defines the energy and momentum distribution of these excitations beyond the Coulomb screening length (\sim 1.5 nm) away from a surface or interface. The electronic bands are likely to deviate strongly from a free electron model at least because they undergo Bragg diffraction at zone boundaries to open band gaps. The spectra in Fig. 7 illustrate the power of momentum mapping spectroscopy.

5. Plasmonic photoemission

We claim that beyond the four plasmon-to-single particle decay channels in section II (a-d), one should also consider the plasmonic photoemission process [41,43–45]. In this decay channel in silver, a collective plasmon mode decays to excite an e-h pair specifically from E_F . Linear photoemission can intrinsically occur by this process only if the work function of a metal is below its bulk plasmon energy. In the case of silver, this requires reduction of the work function by adsorbate modification of the vacuum potential, as has been done in the past [50,51,159,163,231]. It can and does occur for clean single crystal silver surfaces by a nonlinear two plasmon decay process. This is a highly desirable hot electron generation channel, which we rediscovered for the bulk plasmon excitation at Ag single crystal surfaces, because the plasmon energy is not democratically distributed between the electron and hole, but rather the electron retains most of the plasmon energy so that it can drive subsequent chemical or electronic processes. There is strong evidence that this is the common plasmon decay channel [43], but it needs to be recognized and broadly investigated for different materials and various plasmon modes. Plasmonic photoemission has a long history, and our contribution is to have rediscovered it in Ag, gave it a name [41], and documented its historic recognition in the literature [47,48,50,51,231,232]. This experimental research stimulated its modern theoretical description by Gumhalter and Novko [41,43,44,46], which is described in the companion article in this issue of Progress in Surface Science [52].

a. History. Plasmonic photoemission is well established in the literature. Linear plasmonic photoemission has been established by experiment in photoemission spectra of alkali atoms [47,48,233]. When the plasmon resonance energy is above the vacuum level of a metal, as is the case for alkali atoms, the photoemission spectrum gives direct characterization of the products of plasmon decay into single particle excitations. For alkali metals, the hot electron generation was shown to preferentially occur from E_F . Photoemission spectra of alkali atoms show that light exciting their bulk plasmon mode decays to excite e-h pairs such that electrons excited above E_V are photoemitted, enabling their energy analysis. Indeed, such measurements were performed by Smith and coworkers on alkali metal films showing preferential electron emission from E_F [47,48]. Because these experiments were performed before plasmonics became popular, it has failed to impact the thinking and discussion in the plasmonics community.

The plasmonic photoemission from alkali atom films and alkali atom modified Ag surfaces captured the interests of theoreticians [231]. The photoemission spectroscopic studies by Phillips showed that for alkali atoms, and Ag surfaces that had lowered work function by alkali atom adsorption, the excitation of the bulk plasmon mode led to linear photoemission preferentially from the Fermi level [231]. J. J. Hopfield performed calculations beyond the random phase approximation that describe dynamic screening effect on phonon and disorder induced optical absorption leading to photoemission. He found that the photoelectron spectra exciting the bulk plasmon mode of alkali atoms do not produce rectangular distributions, as expected in II.b, but rather distributions that are peaked at $E_F + \hbar \omega_P$ [49]. He further speculated that similar electron distributions may be excited in more complex metals such as Ag.

Such photoelectron distributions have indeed been reported for Ag. Single crystal silver surfaces, were among the first samples to be investigated by nonlinear 2PP, where two-photon transitions overcome the work function barrier [232]. Such measurements were initially performed with nanosecond tunable UV laser excitation [234]. Giesen *et al.* investigated the spectroscopy of Ag(111) surface states as they tuned the excitation light through the IP1 \leftarrow SS resonance [232]. Surprisingly, they found three states that emerged approximately from the IP1 \leftarrow SS resonance, two which tuned with slopes of two and one, in the sense as shown in Fig. 5, and one that hardly tuned, as one might expect for a final state that is fixed by the band structure of the sample [232]. Such state tunings are shown in Fig. 1b of the Gumhalter and Novko review for the low index surfaces of Ag [52]. The tuning states could immediately be attributed to the initial SS and the intermediate IP1 states, but the nontuning state could not be attributed to a final state, because none was predicted at the energy of emission by theory. Giesen *et al.* instead attributed the nontuning state to an Auger process where two electrons promoted to the IP1 state scatter deactivating one to E_F , while the other is emitted with two quanta of the IP1 energy [232]. Because the nontuning state appears very close to the IP1 \leftarrow SS resonance condition, such assignment was plausible. Nevertheless, such Auger process must have a quadratic dependence on the IP1 state population, but this was not tested, and it does not appear to be the case. The nontuning state appears with approximately the same relative intensity to the IP1 state populations must be orders-of-magnitude different.

Later the plasmonic photoemission in linear excitation reappeared in research by Barman *et al.*, who investigated the multipole plasmonic response in single crystalline adlayers and single crystal Ag surfaces with alkali atom-reduced work functions. They performed angle and energy resolved constant initial state photoyield spectroscopy from 2.7 to 18 eV with the goal of characterizing the energy dependence of the multipole plasmon response of Ag [50,51]. Scanning the excitation photon energy through ω_p , while recording photoemission from E_F , they found a strongly enhanced signal at $E_F + \hbar \omega_p$ at 3.80–3.88 eV, consistent with the early spectroscopy of Phillips [231]. While this was the most prominent feature in photoemission from Ag(111) and (100) oriented films, the reason for the enhanced photoyield at $E_F + \hbar \omega_p$ was not scrutinized, as it was not the object of those experiments [50,51].

We have rediscovered the additional nontuning spectroscopic feature in 2PP of Giesen *et al.* [232] by chance when exploring the ENZ response of Ag with femtosecond laser excitation. The frequency onset of the putative Auger peak is the $\epsilon(\omega) = 0$ condition where $\omega = \omega_p$, the bulk plasmon energy of Ag. The plasmonic photoemission appears through a nonlinear promotion of electrons from E_F by

absorption of $2\hbar\omega_p$ energy [41]. Similar multiple plasmon features appear in inelastic electron scattering, but are absent in linear response calculations [235]. We have dubbed the process where ω_p collective polarization decays into e-h pairs at E_F + $\hbar\omega_p$ as plasmonic photoemission, and refer to the nontuning signal peak as the $2\hbar\omega_p$ feature. We also note that second harmonic light emission from silver surfaces has distinct photonic and plasmonic origins, which may be related to the nonlinear plasmonic photoemission [69].

b. The crystal face dependence of plasmonic photoemission. Because the onset of the $2\hbar\omega_p$ feature coincides with the ENZ region, and it cannot be attributed to any single particle properties of the band structure of Ag, we realized that appearing in the ENZ region this must arise from a collective plasmonic response of Ag, and therefore should be common to its other low index surfaces. Note that the $2\hbar\omega_p$ feature attains the maximum intensity < 0.1 eV below the IP1 \leftarrow SS resonance, contrary to what one would expect of an Auger process. This is indeed the case, as can be seen in Fig. 1 of the review by Gumhalter and Novko [52]. Moreover, the $2\hbar\omega_p$ feature also appears on the Ag(110) surface, for which the IP1 state is strongly damped, and not observed because of its coupling with the U_{sp} band [45,236]. The indicated $2\hbar\omega_p$ feature peaks cannot be attributed to the quasiparticle band structure of Ag, but they do not appear at identical energies for all three surfaces [43]. This can be expected because the Fermi surface of Ag (Fig. 3) is not spherical, and thus one can expect a crystalline orientation dependence of the bulk plasmon response.

c. Ag(111). The nonlinear plasmonic photoemission signal of single crystal silver was first observed by Giesen *et al.*, but its assignment was attributed to the plasmonic response by Reutzel *et al.* [41]. Fig. 8a shows a series of one-color 2PP spectra of Ag(111) for different excitation laser frequencies $\hbar\omega_L$ that are tuned through ENZ or $\hbar\omega_p$ [41]. One sees peaks that can be attributed to resonant two photon excitation from the bulk L_{sp} to U_{sp} . Because these are the bulk 3D *sp*-bands, and k_{\perp} momentum is not conserved in photoemission at a surface, the available phase space for the transition is large, but as can be seen from the spectra, it occurs within a narrow spectral region. It is significant that this bulk transition essentially disappears above ~ 3.9 eV, even though in 1PP spectra it persists undiminished over a much wider energy range of comparable final states that are accessed by two photon excitation [224]. Its strong intensity dependence on $\hbar\omega_L$ can be understood from the localized multipole plasmon response of Ag that reaches a maximum between $\hbar\omega_{SP}$ and $\hbar\omega_p$ [237]. Although the resonance condition is available throughout the investigated $\hbar\omega_L$ range, its intensity strongly varies likely because the excitation frequency defines the local field strength, and therefore the nonlinear photoemission response. Simply, the L_{sp} electrons are involved in the multipole plasmon response that screens the optical field and sets up an intensified local field, that drives the nonlinear photoemission process [151].

In addition to the bulk spectral features, the 2PP spectra also probe the surface IP1 \leftarrow SS transition, which has a single-photon resonance at $\hbar\omega_L=3.92$ eV [41]. The resonance enhancement of the IP1 \leftarrow SS transition is clearly observed, but nevertheless both the SS and IP1 peaks appear as separate peaks even under nonresonant conditions. That SS appears in nonresonant two-photon transition is expected, because the initial state is occupied and intermediate state in two-photon absorption can be virtual. Why the IP1 band appears under nonresonant conditions is more perplexing and requires additional research. According to its broad $k_{||}$ dispersion, the initial state for its excitation cannot be the SS, which is occupied only over a limited $k_{||}$ range. Angle resolved spectra in Fig. 9 show evidence for IP1 \leftarrow L_{sp} excitation under resonant conditions. Because only L_{sp} can provide the observed $k_{||}$ range to populate the IP state, and the fact that it is strongly detuned from resonance, suggest that the IP state excitation involves a many body response. One can certainly anticipate that the transient exciton and non-Markovian response of Ag(111) that involves a time dependent screening of photoexcited electron charge has some role in enhancing 2PP via the nonresonant excitation of the IP1 state [221,238],

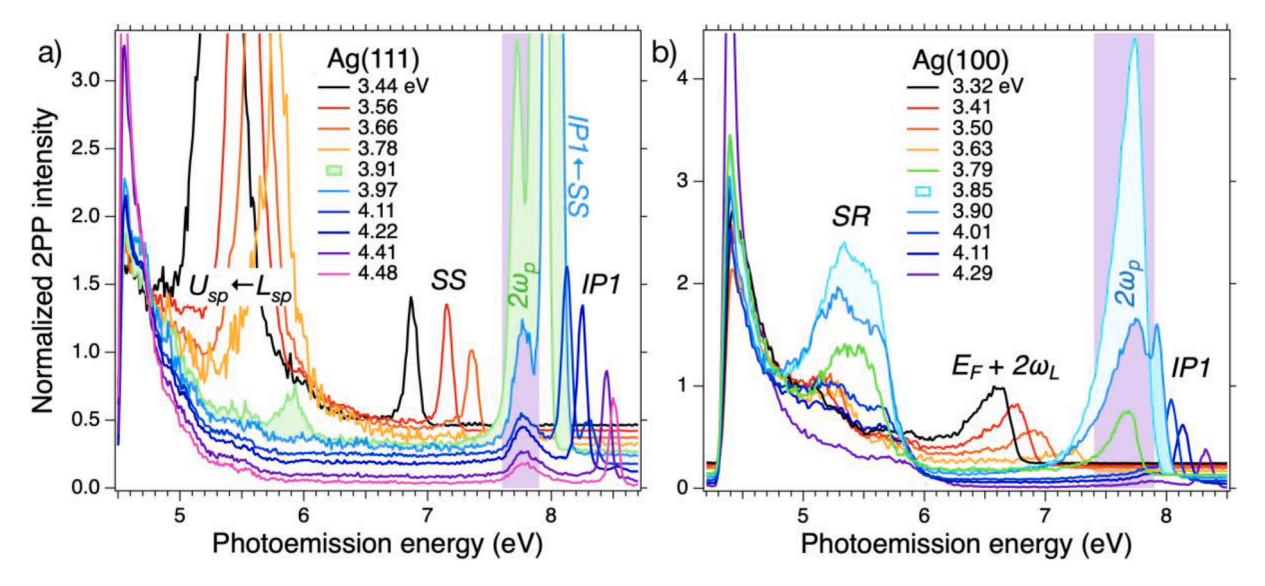


Fig. 8. A) 2PP spectra of Ag(111) through the $\hbar\omega_p$ resonance at $\hbar\omega_L = 3.91$ eV (shaded green). The spectra are normalized at the E_V edge except for the $\hbar\omega_L > 4.4$ eV, which are normalized at $E_{fin} = 4.8$ eV because of strong 1PP contribution at the E_V edge. The $E_F + 2\hbar\omega_p$ feature region is highlighted by purple background. Assignments of specific interband transitions are indicated in the prominent spectral regions. Adopted from Ref. 41. (For interpretation of the references to color in this figure legend, the reader is referred to the web version of this article.)

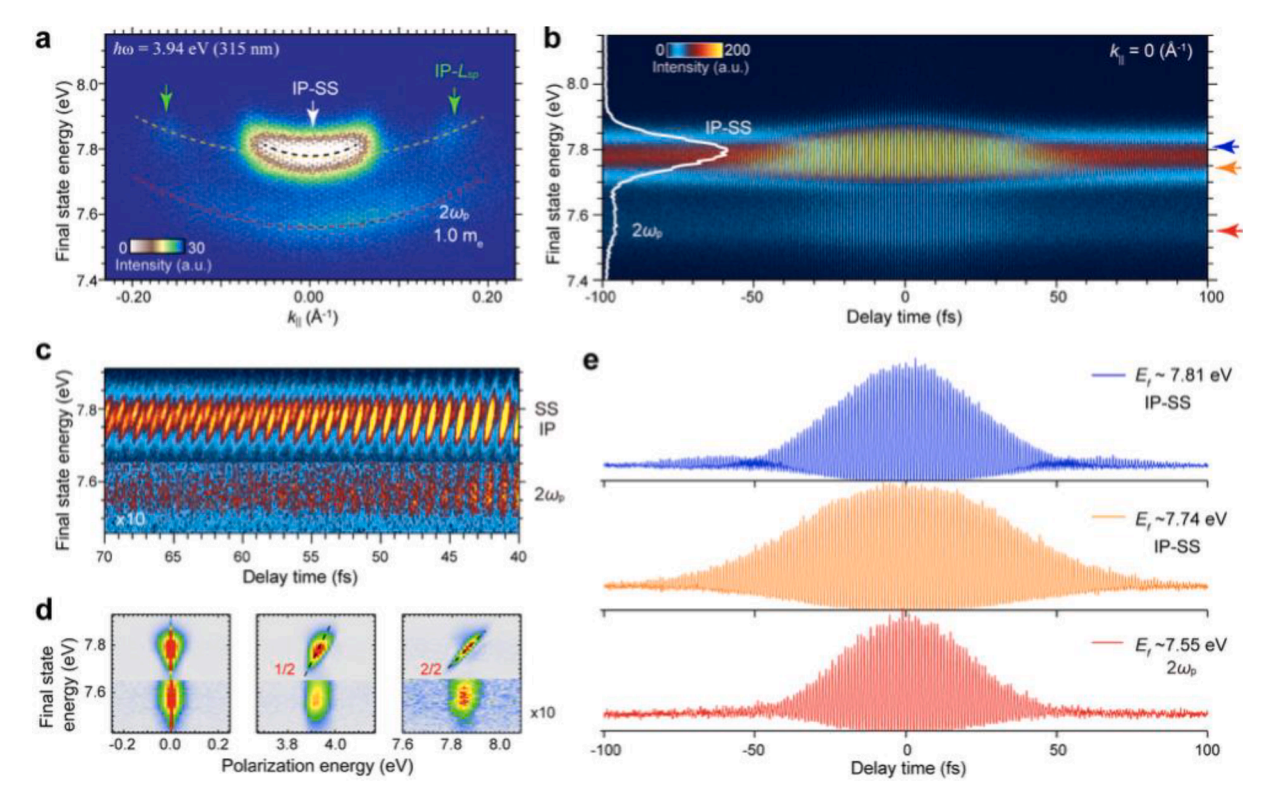


Fig. 9. ITR-2PP measurements of coherence in 2PP processes in two-photon single particle IP \leftarrow SS and collective $2\hbar\omega_p$ feature excitations at ENZ. a) 2PP spectrum showing the dispersive $2\hbar\omega_p$ feature, the nearly resonant IP-SS transition, and resonant IP \leftarrow L_{sp} transition. ITR-2PP data are taken by recording 2PP spectra as a function of delay between two identical excitation pulses with interferometric delay scanning. b) The $k_{||}$ =0 Å⁻¹ slice through the 3D ITR-2PP data. The white line shows the line profile through the data at τ = 0 fs, showing the near resonant IP \leftarrow SS transition signal and the $2\hbar\omega_p$ feature. c) Enlarged region of the ITR-2PP measurement showing tilting of the coherent fringes for the IP-SS transition, which are nearly vertical for the $2\hbar\omega_p$ feature, consistent with an incoherent nonlinear excitation process. d) Fourier transform spectral components of the data in b) at the 0ω , 1ω , and 2ω components of the driving frequency. The IP and SS signals tilt with the indicated slopes, as expected for a coherent process, while those of the $2\hbar\omega_p$ feature hardly show a tilt. e) Line profiles of the data in b) at energies indicated by the colored arrows. Extended dephasing times are recorded at 7.81 and 7.74 eV, respectively following the SS and IP coherence in near resonant IP \leftarrow SS excitation. By contrast, the $2\hbar\omega_p$ feature the interference fringes follow the field of the excitation pulses. This is consistent with a correlated $2\hbar\omega_p$ feature evolving into a single particle photoelectron.

but this requires further study.

While the bulk and surface band features have been correctly assigned from the infancy of 2PP spectroscopy [232], the abrupt appearance of the $2\hbar\omega_p$ feature at $\hbar\omega_L=3.9$ eV cannot be explained by the single particle band structure of Ag. The [111] projected band gap in which the plasmonic photoemission is observed is indicated by ellipse "1" in Fig. 3. Note that a thermomodulation study at 100 K locates one-photon interband L_{sp} to U_{sp} transition at $\hbar\omega_L=3.88$ eV, and d-band to L_{sp} transition [159] at $\hbar\omega_L=4.04$ eV [239], neither one of these processes can explain the $2\hbar\omega_p$ feature over the investigated $\hbar\omega_L$ range. As $\hbar\omega_L$ is tuned past $\hbar\omega_p$, the $2\hbar\omega_p$ feature rapidly decreases in intensity, and gradually shifts to a modestly higher energy, but with a noninteger slope of 0.29. This shift cannot be attributed to a photon order of photoemission of a single particle state, but could be related to the dispersive transverse plasmon k_\perp dependence of coupling above ENZ; the required perpendicular momentum can be supplied by the nonlocal dielectric response of the metal surface [57,240].

A further aspect of the $2\hbar\omega_p$ feature is its $k_{||}$ dispersion. This is doubly surprising because: 1) the Fermi level, from which photoemission occurs, is in a projected band gap of Ag(111), so there is no L_{sp} DOS at the Fermi level at $k_{||}=0$ Å $^{-1}$, from which a single particle could be excited to a final state at $E_F+2\hbar\omega_p$; and furthermore, 2) $k_{||}$ appears to be a good quantum number. The photoemitted electrons must come from other parts of the Brillouin zone, presumably involving some momentum transfer, and yet the $2\hbar\omega_p$ feature still possesses $k_{||}$ dispersion corresponding to a free electron with an effective mass, $m=-1m_e$. This effective mass is consistent with the electron optical mass at E_F [122]. The fact that the $2\hbar\omega_p$ feature implies excitation of electrons that do not exist in a single particle band structure, points to its collective character. In fact, correlation effects can produce satellite features in photoemission spectra that cannot be attributed to single particle band structures [241]. For example, such a collective excitation could be plasmaron, a composite particle of plasmon and electron [62,242,243]. The screened Coulomb interaction, $V(q)/\epsilon$, where q is a wavevector, defines the plasmaron quasiparticles formation [244]. Because we detect this response in the ENZ ($\epsilon=0$) region, one should expect the plasmon-electron interaction to be particularly strong, such that plasmaron spectroscopic features may be anticipated.

We further note that the $2\hbar\omega_p$ feature has probably appeared in UV survey spectra of IP states of Ag(111). For example, in Fig. 22 of Ref. [245], an extra spectroscopic feature appears between the IP1 and IP2 states, but there it is neither mentioned nor assigned. While the single particle band structures of silver are well understood by experiment and theory, spectroscopy at ENZ shows evidence of collective responses that are not yet understood.

d. Ag(100). Next, we examine the plasmonic response of the Ag(100) surface. The spectra from Marks in Fig. 5 use UV photon energy that is significantly above $\hbar\omega_p$, where a plasmonic signal is not expected. Fig. 8b presents 2PP spectra of Ag(100) when $\hbar\omega_L$ is tuned through $\hbar\omega_p$. These spectra show similar features to Fig. 5 mainly reflecting the excitation of intermediate unoccupied states, except 1) for excitation at $\hbar\omega_L = \le 3.50$ eV, there is strong two-photon excitation from the E_F ; and 2) at $\hbar\omega_L = 3.85$ eV there is an abrupt onset of plasmonic photoemission. The [100] projected band gap in which the plasmonic photoemission is observed is indicated by ellipse "2" in Fig. 3 and is evident in the band structure of Fig. 2. Again, the plasmonic peak tunes with 0.29 $\hbar\omega_L$ for excitation above its onset, and rapidly drops in intensity. The two-photon excitation from E_F has considerable intensity gained by the surface character of a broad Shockley surface resonance located at ~ 1.3 above E_F [226]. The considerable width of this resonance makes its low energy wing partially occupied below E_F [32]. As in the case of Ag(111), the bulk features of Ag(100) associated with two-photon excitation from E_F disappear as $\hbar\omega_L$ approaches $\hbar\omega_p$. Again, we attribute this to the diminished role of the E_{SP} electrons in screening of the optical field. It is noteworthy that the $2\hbar\omega_p$ feature at $\hbar\omega_L = 3.85$ eV has significantly higher peak intensity than the hot electron signal from the surface resonance and the E_{SP} DOS that extends up to $E_F + 2.0$ eV, indicating that it is the dominant nonlinear electronic response.

e. Ag(110). Fig. 6 immediately shows that the surface normal emission of Ag(110) is dominated by hot electrons whose population declines from the E_V edge with energy approximately exponentially over entire 2PP spectra. In addition, at $E_F + 2\hbar\omega_L$ energy there are $2\hbar\omega_p$ features (see also Fig. 1 of the Gumhalter and Novko review), which appear at a slightly lower $2\hbar\omega_L$ than for Ag(111) and Ag(100) surfaces. Unlike the other surfaces, the $2\hbar\omega_p$ feature energies and anisotropies appear to be affected by a minigap in the experimentally determined 7.3–7.7 eV range (predicted at 7.0–7.3 eV in the band structure of Ag(110) in Fig. 2), which supports an unoccupied surface state. The bulk band curvatures from where the photoemission occurs are highly asymmetric, as can be seen in the [110] projected bands that are indicated by ellipse "3" in Fig. 3. We believe that this surface state and the anisotropy of the bulk bands from which it derives, define the anisotropy of the Ag(110) plasmonic photoemission [123,240,246].

That these plasmonic responses are highly anisotropic can be seen from their exceptional polarization dependence and dispersions that appear to be related to the atomic scale corrugation and anisotropy of this surface. This structural anisotropy additionally generates a reciprocal space anisotropy of the electronic bands, that distinctly define this surface. Whereas when the the [001] direction is in the optical plane, Fig. 6 shows the expected, or normal, p-polarization dependence of the plasmonic response. The surface normal field component enhances the plasmonic response, as well as the hot electron signal component. By contrast, when the excitation is performed with the $[1\bar{1}0]$ direction in the optical plane, the surface parallel component dominates the plasmonic response, opposite to the hot electron signal. We believe that this could related to the two-atom corrugation of the (110) surface in the [001] direction (Fig. 7c), but it could also be related to the surface state character of the final state, and transition moments for its excitation. It definitely contradicts the common assumption [154] that hot electron excitation by Drude absorption and by decay of plasmons follow the same physics that are described in Sections II.a-d. Specifically, the opposite polarization dependence of the plasmonic photoemission and hot electron signal shows that the hot electron component is not generated by the bulk plasmon decay, and that the two modes couple to the surfaces through different physics. The electronic anisotropy of the (110) surface is pictorially evident in the momentum microscope 3D photoemission spectrum in Fig. 7, where the plasmonic photoemission signal is designated as S3. The anisotropy of this signal arises from effective masses of the bulk bands, and consequently the surface, at the final state energy for the $2\hbar\omega_p$ feature [43]. Such highly anisotropic response is fully in agreement with the calculated plasmonically induced transitions by Gumhalter and Novko in their Figs. 5 and 6 [52]. The 3D momentum microscope spectrum in Fig. 7 also shows a strong anisotropy of the surface and bulk transition of the (110) surface, that appear to be a common feature of (110) surfaces of noble metals [247].

f. Plasmonic photoemission from other modes and metals. The plasmonic photoemission through coupling to the bulk plasmon mode of silver single crystal surfaces is firmly established in the above experiments on Ag(111), (100) and (110) surfaces [43]. One may ask whether this is a peculiarity of silver, or of nonlinear photoemission from bulk plasmon modes of single crystal surfaces. For example, other metals have plasmonic responses, and depending on the sample structure and excitation process, there are also the LSP and SPP responses. For example, there is no evidence of plasmonic photoemission from free electron metals like Al and Be, which have bulk plasmon responses in the VUV, and have extensively been investigated [57,248–250]. We have already recalled the history that in the case of alkali metals, linear excitation of plasmon modes preferentially excites photoemission from E_F [47,48,233]. There is, however, increasing evidence that the nonlinear variant of plasmonic photoemission is more broadly observed in experiments that are capable of analyzing the primary decay pathways of plasmons into single particle excitations.

For example, Shibuta et~al. examined the decay of the LSP mode of size selected Ag clusters on semiconducting C_{60} overlayers, and discovered that clusters as small as Ag₉ emit electrons approaching the $E_F + 2\hbar\omega_{UV}$ energy upon excitation of the LSP mode with UV light [251]. Their interpretation is that the LSP mode of Ag_n clusters decays into hot electrons at $E_F + \hbar\omega_{UV}$ energy, which are then detected by photoemission with another UV photon. This emission process becomes stronger for larger clusters presumably because they acquire better defined plasmon response. The maximum of this response occurred between $\hbar\omega_L = 3.31$ and 3.96 eV, but their laser could not be tuned between that interval to obtain an exact value for the enhancement. Their experimental time resolution of ~ 100 fs was insufficient to evaluate the hot electron generation and relaxation dynamics, but apparently a highly energetic hot electron distribution from plasmon decay promoting electrons from E_F could be captured.

In another experiment Hartelt *et al.* and Dreher *et al.* examined the hot electron distribution in a two-quantum decay of the SPP mode of polycrystalline Au sample. This was a challenging experiment, because it required the isolation of the two-quantum SPP mode

process from that where one excitation quantum from the SPP mode generates a hot electron, and the other quantum from an optical probe pulse photoemits it. Again, these researchers found that two SPP quanta preferentially excite photoemission from E_F , generating a signal correlating with $E_F + 2\hbar\omega_{\text{SPP}}$, where ω_{SPP} is the generated SPP frequency [252–254]. This is particularly surprising because Hartelt *et al.* used a polycrystalline sample [252] which has crystallites of various orientations.

From these reports we conclude the plasmonic photoemission from silver is a more broadly observed process in both alkali atoms and noble metals, and can be a consequence of excitation of other plasmon modes; therefore, when discussing plasmonically-induced hot electron processes it is essential to have an actual measurement of the hot electron distribution, rather than to assume a hot electron distribution based on untested or oversimplified theoretical models.

6. Plasmonic photoemission dynamics

Plasmonic photoemission $2\hbar\omega_p$ feature signals appear along with the surface and bulk interband transitions of Ag, as can be seen in the spectra of the single crystal surfaces (Fig. 1 of the accompanying Gumhalter and Novko publication [52] and Fig. 9, here). One may wonder whether ultrafast coherent spectroscopy can provide further information on the plasmonic photoemission process. Such measurements are performed by the interferometric time-resolved 2PP (ITR-2PP) method [37,157,163,255], and analyzed according to procedures that have been applied to mPP processes [39]. The measurements are angle (k||) resolved, and thus, they can probe the decoherence of photoexcited eigenstates [39]. The available coherent interactions are particularly useful in exploring Floquet engineering of electronic band structure at PHz frequencies [256]. These are some advantages over the commonly performed angle and time resolved photoemission measurements that are commonly applied to quantum materials [202]. ITR-2PP measurements are performed for excitation near (above) the $\hbar \omega_p$ frequency, where the $2\hbar\omega_p$ feature appears in 2PP spectra. Fig. 9a shows 2PP spectra recorded with $\hbar\omega_L=3.94$ eV for Ag(111) surface, which is near the IP1 \leftarrow SS resonance that dominates the signal. The bright signal that extends over the $|k_{||}|=0.07 \text{ Å}^{-1}$ range matches the occupied region of SS, because it is enhanced by near resonance with the IP1 state. Correspondingly, the IP1 state is bright predominantly in the occupied region of SS, signifying that SS is the initial state for the excitation of the IP1 state in this momentum range, and that photoemission from IP1 occurs faster than its dephasing. Nevertheless, IP1 extends further in k_{\parallel} than SS, and its intensity is enhanced at $|k_{\parallel}| = \sim 0.16 \text{ Å}^{-1}$. We attribute this to resonance enhanced excitation of IP1 from the occupied bulk L_{sp} band, from initial states where it approximately crosses E_F . The dashed curves superposed on Fig. 9a at the IP1 and $2\hbar\omega_p$ features display dispersions corresponding to $m_e = 1$.

Fig. 9b shows an ITR-2PP measurement at $k_{||} = 0$ Å⁻¹ that is extracted from a 3D data set of photoelectron counts $vs. E_f(k_{||}, \tau)$. The ITR-2PP data are taken with two identical pump-probe pulse excitation, where their delay τ is scanned in ~ 100 as steps, while 2PP $E_f(k_{||})$ spectra excited by their joint action are recorded at each delay interval. The data show signal that again is dominated by the IP1 \leftarrow SS resonance at ~ 7.80 eV and below it the $2\hbar\omega_p$ feature appears at ~ 7.55 eV. The vertical line profile at pulse delay $\tau=0$ fs shows the 2PP spectrum at $k_{||}=0$ Å⁻¹, where the dominant IP1 \leftarrow SS and weaker $2\hbar\omega_p$ feature peaks appear. An enlarged portion of the ITR-2PP data is shown in Fig. 9c for the $\tau=70$ –40 fs range where three sets of interference fringes can be seen. The top two sets belong to the near resonant IP1 \leftarrow SS transition where SS appears moderately (~ 0.05 eV) above IP1. The fringes are separated in part because energy resolution of the experiment increases as τ increases. In other words, as expected from the energy-time uncertainty, the frequency width excited by of the pulse pair decreases as τ increases, as long as the coherence between SS and IP1 persists [3]. The fringes follow hyperbolic tilting [257] with increasing delay that portends a coherent process involving homogeneously broadened levels [39]. This can further be evaluated by taking a Fourier transform (FT) of the ITR-2PP signal for $k_{||}=0$ Å⁻¹, which is shown in Fig. 9d. The FT spectra are reported for signals oscillating from 0ω to 2ω of the driving frequency. Like the tilted fringes, the FT spectra at the SS and IP1 energies tilt with slopes that are defined by the polarization frequency/photoemission order, for example, indicated by slopes $\frac{1}{2}$ and $\frac{1}{2}$ 0 in Fig. 9d.

Fig. 9c also shows fringes for the $2\hbar\omega_p$ feature, which are hardly tilted in the time domain, that consequently produce FT spectra that hardly show a tilt. Moreover, the coherent fringe amplitudes of the $2\hbar\omega_p$ feature decay much faster than those of the SS and IP1 signals, as can be seen in the line profiles through the ITR-2PP data in Fig. 9e. The faster fringe decay is consistent with a faster dephasing, but if the excitation process were coherent, it would still have tilted FT spectra, albeit that are broader in frequency [258]. The untiled spectra, instead, portend that the $2\hbar\omega_p$ feature involves an incoherent process that is involved in generation of the signal at $E_F + 2\hbar\omega_L$ at $k_{||} = 0$ Å⁻¹ when neither the initial nor the intermediate single particle bands can exist within the projected band gap of Ag (111). For example, assuming that the $2\hbar\omega_p$ feature is excited from a correlated many-body state, for example a plasmaron, promotion of electron to an excited state may extinguish the correlation causing the coherence to be lost. Moreover, the bulk plasmon is excited in the near surface region, suggesting that the nonlocal plasmon screening response can excite a range of wave vectors that evolve at different frequencies.

7. Conclusions

This review summarizes the collective and single particle, coherent and incoherent, nonlinear photoemission responses of silver in the UV near its ENZ bulk plasmon response. We have presented an experimental overview of the plasmonic photoemission, as a companion article to summarize the experimental research that stimulated the theoretical description of related process by Gumhalter and Novko [52], as well as the related hot electron generation in Ag single crystal surfaces near ENZ. The collective plasmon responses of silver have been extensively investigated in the multipole, the surface polariton, and at the bulk plasmon resonances by inelastic electron scattering methods [149,259–262]. Although silver is a popular and prototypical plasmonic material, its single particle and collective responses have hardly been investigated in a comprehensive manner as a function of the excitation photon frequency,

crystalline orientation, and from the perspective of excitation transfer between the single and collective mode responses, with some notable exceptions [6,59,97,122]. Silver has a particularly sharp and well-defined plasmonic response among noble metals, but its fully occupied d-bands cause some notable deviations from the free electron plasmon model [122]. Therefore, it is not clear to what extent the plasmonic responses reported here can be transferred to other metals.

We have reviewed the available studies of plasmonic photoemission, where at, or above the $\hbar\omega_L \ge \hbar\omega_p$ frequency, the optical polarization of the plasmonic response leads to non-Einsteinian excitation of electrons from E_F [41,43]. This process is non-Einsteinian in the sense that instead the optical field exciting electrons directly, as it does below $\hbar\omega_p$, at and above $\hbar\omega_p$, in the linear regime, a component of the signal is generated by an internal field at ω_p that subsequently excites electrons specifically from E_F by $\hbar\omega_p$. Interferometric measurements in Fig. 9 show that the behavior of the external and internal fields on driving the coherent response are distinct from single particle excitations. Although the plasmonic photoemission has been established most unequivocally for single crystal Ag surfaces, related responses have been reported in Ag nanoparticles [251], and for SPP modes on polycrystalline Au surfaces [252]. Moreover, similar photoemission processes have been described for alkali metals [47,48,233], and alkali atom modified single crystal silver surfaces [50,51], as well as having been predicted by theory [17,44,49,233]. The significance of plasmonic photoemission and related collective-to-single particle decay processes to the field of plasmonics is that the primary plasmon decay process deposits the plasmon energy entirely into single particle excitations, rather than distributing it between electron and hole [41,43]. This unanticipated outcome may be relevant to explaining the claimed efficiency of many plasmonic phenomena, and encourages research that actually tests the single particle energy–momentum distributions from plasmonic decay rather than casting them into models that are unproven by experiment, and rely on oversimplified theory.

We have also considered hot electron generation in Ag, to specifically address the broadly used models for hot electron generation through Drude intraband absorption or plasmon decay. The broadly applied models for hot electron generation rely on free electron models that assume spherical energy–momentum distributions far away from E_F . A cursory glance at elemental Fermi surfaces in the Florida State University compendium [214] shows that such assumption of spherical surfaces is possibly only valid for the alkali atom group, for which it has also been well established that plasmonic excitation promotes electrons from E_F [47,48,233]. Although noble metal Fermi level surfaces approach the spherical symmetry of alkali atoms, with the exception of neck formation at the Bragg planes in the [111] direction. Fig. 3 shows that this departure from isotropy grows with increasing energy, so that the assumption of an isotropic surface is invalid at eV energies above E_F in considering how hot electron generation can induce photochemical or photovoltaic processes. Only the (110) surface of Ag provides rich evidence for hot electron generation in the E_F - E_V energy range [45]. To the extent that hot electrons are generated by intraband processes, they are likely to assume highly anisotropic distributions that depend on their energy. The threshold energy of interband energetic electron generation in Ag is defined by L_{sp} to U_{sp} transition at $\hbar\omega_L$ = 3.88 eV [239], though there is scant evidence for the electronic population of the U_{sp} band [263].

While mPP spectroscopy of single crystal Ag surfaces provides many details of single particle excitations through direct or plasmonic intraband and interband transitions, there are many aspects of the presented results that remain unexplained. While linear and nonlinear photoemission spectroscopies are powerful methods to evaluate the band structures and quasiparticle dynamics of complex solids where electron–electron, electron–phonon, and other interactions play important roles [202,264], one would hope that it is possible to unravel the complex dynamics that affect the nonlinear photoemission from noble metal surfaces. Some aspects of the presented research that require further experimental and theoretical investigation follow.

- 1) Nonlinear plasmonic photoemission: While theory predicts that plasmon decay excites electrons preferentially from E_F , details of how this happens are not fully established beyond the theory of Gumhalter and Novko [44,46,52]. In the case of Ag(111) there are no states at E_F in the band gap, yet a dispersive photoemission signal is observed. Although SS is 0.065 eV below E_F , it cannot be the initial state for this process, because the dispersive $2\hbar\omega_p$ feature extends beyond the $k_{||}$ range where SS is occupied. Moreover, the Fourier transform data in Fig. 9d are not consistent with the response at ω_p acting as a polarization field, where two or more quanta decay to excite a single e-h pair. Instead, it is more consistent with plasmonic photoemission originating from a correlated plasmon-electron state that forms through enhanced Coulomb interaction at ENZ, or plasmaron, which decays upon electron promotion to the vacuum state. The theory of Gumhalter and Novko is a departure from previous descriptions of light-matter interaction on the ultrafast time scales in that it explicitly considers the role of the applied field in interactions with the collective plasmonic response and in nonlinear optical processes that approach the nonperturbative regime [52]. The goals of their and our reviews are to promote new thinking and research on how plasmonic excitations mediate the light energy transduction in plasmonic metals.
- 2) The enhancement of plasmonic photoemission from Ag(110) when the crystal is held with the $[1\bar{1}0]$ axis in the optical plane is highly unexpected to be maximum with s-polarized excitation. One would think that the non-local dielectric response that can couple into the bulk plasmon mode to require an optical field that is surface normal, rather than to be maximum for the in-plane excitation field. Because the surface is corrugated in the [001] direction into which the field points, one can argue that the surface parallel field drives, in addition, a surface normal response. Considering that the corrugation is on the atomic scale, while the driving field wavelength is ~ 330 nm, this is highly surprising. One should, however consider other factors. In case of the Ag(110) surface, one should realize that the transition terminates in a peculiar strongly dispersive surface state within a minigap, rather than belonging to the photoemission continuum. This surface state is also peculiar in that its maximum DOS is in the second atomic layer from the surface [265]. While this photoemission process has plasmonic character, it can also have single particle character, so to understand the preference of s-polarized excitation one should also consider transition moments for the L_{sp} to U_{sp} two-photon transition.

- 3) The $2\hbar\omega_p$ feature spectra for the Ag(111) surface are skewed towards high frequency region, while those of the Ag(100) and Ag (110) are skewed to the low frequency. Such lineshape skewing can arise if the 2PP process via these collective excitations is accompanied by low frequency bosonic *e-h* pair excitations associated with the screening of the applied field and the created electron and hole final states [238]. The lineshapes can also have an inhomogeneous component due to a broad momentum distribution that participates in the nonlocal screening of the optical field. Currently, however, there is no concrete theoretical explanation for the $2\hbar\omega_p$ feature skewing in the case of Ag surfaces.
- 4) The skewing of the lineshapes, and the slope of the $2\hbar\omega_p$ feature vs. $\hbar\omega_L$ of 0.29 may be related. This slope could be caused by the k_{\perp} dispersion of the transverse bulk plasmon response, which was invoked to explain the constant initial state photoemission spectra of free electron metals [57]. The slope of the $2\hbar\omega_p$ feature is the same for all three surfaces within the accuracy of the measurement.
- 5) The nonresonant IP state excitation in noble metals, and specifically in Ag has never been fully understood. In Fig. 8, the IP1 intensities under nonresonant conditions do not follow a dependence on $\hbar\omega_L$ that one would expect from the simple detuning from resonance with SS. Moreover, the IP1 momentum distribution is broader than the occupied SS occupation, so a simple near resonance argument does not work. In Fig. 9a there is evidence for a coherent resonant IP $\leftarrow L_{sp}$ transition that populates the high $|k_{||}|$ states. It has been argued that incoherent transfer from U_{sp} can populate IP1 [266,267], but this apparently does not happen in experiments that can probe such excitation [263]. In considering how the IP states get populated, one must remember that they are not preexisting states, but rather form in response to screening of an electron charge at a metal surface, which happens typically on sub-femtosecond time scale [221,222]. Thus, the IP state population may be defined, in part, by this screening response.

To summarize, while time-resolved photoemission techniques are being applied to complex correlated and topological materials [202,268], it is useful to investigate seemingly simple noble metal systems. It helps to build up an understanding of coherence and correlation in light-matter interactions for relatively well understood materials, like noble metals, to be able to apply such experimental methods with confidence to more complex materials. It is clear that as the time resolution of the performed experiments reaches into the attosecond regime [256], it is important to have a thorough understanding of the electron correlation that is introduced by the pumping and probing optical fields. Moreover, the excitation light cannot be simply considered as such that propagates through the vacuum, but one must consider how it is affected by response of the electronic system with which it interacts [41,44,52,203,222,269]. One should also recall that optical fields not only carry energy, but also spin and OAM that can induce chiral and biansiotropic interactions that break the time-parity symmetry to introduce nonreciprocity [106,108,270–272]. The paradigmatic plasmonic response of Ag as exemplified by its ENZ response is ideal to build on its complexity to explore correlated electronic responses on ultrafast time scales.

Declaration of Competing Interest

The authors declare that they have no known competing financial interests or personal relationships that could have appeared to influence the work reported in this paper.

Acknowledgements

The authors thank B. Gumhalter and D. Novko for continued collaboration on the theory of plasmonic photoemission and related phenomena, and specifically for incisive comments on this review, as well as providing the Figs. 2 and 3. HP thanks Sean Garret Roe for searching for old 2PP survey spectra of Ag(111) and Dino Novko for performing the calculations that are reported in Figs. 2 and 3. This research was partially supported by DOE-BES Division of Chemical Sciences, Geosciences, and Biosciences Grant No. DE-SC0002313, and NSF grant CHE-2102601. S.T. acknowledges the support from CAS Project for Young Scientists in Basic Research (YSBR-054) and the National Natural Science Foundation of China (21972129, 11904349). MR acknowledges his Feodor Lynen postdoctoral support through the Alexander von Humboldt Foundation at the University of Pittsburgh in the group of HP, and the Deutsche Forschungsgemeinschaft (DFG, German Research Foundation) - 217133147/SFB 1073, project B10. AL acknowledges the support from the International Center for Advanced Studies of Energy Conversion (ICASEC) through their International Visitor Program (University of Göttingen), which enabled the momentum microscope experiments in Fig. 7.

References

- [1] R.R. Cavanagh, D.S. King, J.C. Stephenson, T.F. Heinz, Dynamics of nonthermal reactions: Femtosecond surface chemistry, J. Phys. Chem. 97 (4) (1993) 786–798, https://doi.org/10.1021/j100106a002.
- [2] H. Petek, S. Ogawa, Femtosecond time-resolved two-photon photoemission studies of electron dynamics in metals, Prog. Surf. Sci. 56 (1997), 239. http://www.sciencedirect.com/science/article/pii/S0079681698000021.
- [3] H. Petek, M.J. Weida, H. Nagano, S. Ogawa, Real-time observation of atomic motion above a metal surface, Science 288 (2000), 1402. http://www.sciencemag.org/content/288/5470/1402.full?sid=3247dea4-d1be-4c20-8bc5-2529e00a4f85.
- [4] H. Petek, H. Nagano, M.J. Weida, S. Ogawa, Surface femtochemistry: frustrated desorption of alkali atoms from noble metals, J. Phys. Chem. B 105 (29) (2001) 6767–6779, https://doi.org/10.1021/jp0045235.
- [5] X. Zhu, Electron transfer at molecule-metal interfaces: a two-photon photoemission study, Annu. Rev. Phys. Chem. 53 (2002), 221. http://physchem. annualreviews.org;4040/cgi/content/abstract/53/1/221.
- [6] J.M. Pitarke, V.M. Silkin, E.V. Chulkov, P.M. Echenique, Theory of surface plasmons and surface-plasmon polaritons, Rep. Prog. Phys. 70 (1) (2007). http://stacks.iop.org/0034-4885/70/1.
- [7] G.V. Hartland, Optical studies of dynamics in noble metal nanostructures, Chem. Rev. 111 (6) (2011) 3858-3887, https://doi.org/10.1021/cr1002547.
- [8] X. Zhang, Y.L. Chen, R.-S. Liu, D.P. Tsai, Plasmonic photocatalysis, Rep. Prog. Phys. 76 (2013), 046401. http://stacks.iop.org/0034-4885/76/i=4/a=046401.

- [9] J. Li, S.K. Cushing, F. Meng, T.R. Senty, A.D. Bristow, N. Wu, Plasmon-induced resonance energy transfer for solar energy conversion, Nat Photon 9 (9) (2015) 601–607, https://doi.org/10.1038/nphoton.2015.142.
- [10] S.V. Boriskina, et al., Losses in plasmonics: from mitigating energy dissipation to embracing loss-enabled functionalities, Adv. Opt. Photon. 9 (2017), 775. https://opg.optica.org/aop/abstract.cfm?URI=aop-9-4-775.
- [11] U. Aslam, V.G. Rao, S. Chavez, S. Linic, Catalytic conversion of solar to chemical energy on plasmonic metal nanostructures, Nat. Catal. 1 (2018) 656–665, https://doi.org/10.1038/s41929-018-0138-x.
- [12] Y. Zhang, S. He, W. Guo, Y. Hu, J. Huang, J.R. Mulcahy, W.D. Wei, Surface-plasmon-driven hot electron photochemistry, Chem. Rev. 118 (6) (2018) 2927–2954, https://doi.org/10.1021/acs.chemrev.7b00430.
- [13] L.V. Besteiro, P. Yu, Z. Wang, A.W. Holleitner, G.V. Hartland, G.P. Wiederrecht, A.O. Govorov, The fast and the furious: ultrafast hot electrons in plasmonic metastructures. Size and structure matter. Nano Today 27 (2019), 120. http://www.sciencedirect.com/science/article/pii/S1748013219301045.
- [14] T.P. Rossi, P. Erhart, M. Kuisma, Hot-carrier generation in plasmonic nanoparticles: the importance of atomic structure, ACS Nano 14 (8) (2020) 9963–9971, https://doi.org/10.1021/acsnano.0c03004.
- [15] S. Kumar, A. Habib, R. Sundararaman, Plasmonic hot carriers scratch the surface, Trends Chem. (2021). https://www.sciencedirect.com/science/article/pii/ S2589597421001714.
- [16] Y. Zhu, H. Xu, P. Yu, Z. Wang, Engineering plasmonic hot carrier dynamics toward efficient photodetection, Appl. Phys. Rev. 8 (2021), 021305. https://aip.scitation.org/doi/abs/10.1063/5.0029050.
- [17] H. Jin, J.M. Kahk, D.A. Papaconstantopoulos, A. Ferreira, J. Lischner, Plasmon-induced hot carriers from interband and intraband transitions in large noble metal nanoparticles, PRX Energy 1 (2022), 013006. https://link.aps.org/doi/10.1103/PRXEnergy.1.013006.
- [18] O.A. Douglas-Gallardo, C.L. Box, R.J. Maurer, Plasmonic enhancement of molecular hydrogen dissociation on metallic magnesium nanoclusters, Nanoscale 13 (25) (2021) 11058–11068, https://doi.org/10.1039/D1NR02033A.
- [19] H. Petek, Single-molecule femtochemistry: molecular imaging at the space-time limit, ACS Nano 8 (1) (2014) 5-13, https://doi.org/10.1021/nn4064538.
- [20] E. Cortés, R. Grzeschik, S.A. Maier, S. Schlücker, Experimental characterization techniques for plasmon-assisted chemistry, Nat. Rev. Chem. 6 (2022) 259–274, https://doi.org/10.1038/s41570-022-00368-8.
- [21] R.L.M. Gieseking, Plasmons: untangling the classical, experimental, and quantum mechanical definitions, Mater. Horiz. 9 (1) (2022) 25–42, https://doi.org/10.1039/D1MH01163D.
- [22] C.G. Sánchez, M. Berdakin, Plasmon-induced hot carriers: an atomistic perspective of the first tens of femtoseconds, J. Phys. Chem. C 126 (24) (2022) 10015–10023, https://doi.org/10.1021/acs.jpcc.2c02147.
- [23] R. Xue, P. Ge, J. Xie, Z. Hu, X. Wang, P. Li, Controllable CO₂ reduction or hydrocarbon oxidation driven by entire solar via silver quantum dots direct photocatalysis, Small (2023), 2207234. https://onlinelibrary.wiley.com/doi/abs/10.1002/smll.202207234.
- [24] C. Zhang, Y. Luo, S.A. Maier, X. Li, Recent progress and future opportunities for hot carrier photodetectors: from ultraviolet to infrared bands, Laser Photonics Rev. 16 (2022), 2100714. https://onlinelibrary.wiley.com/doi/abs/10.1002/lpor.202100714.
- [25] S. Tan, A. Argondizzo, J. Ren, L. Liu, J. Zhao, H. Petek, Plasmonic coupling at a metal/semiconductor interface, Nature Photon 11 (12) (2017) 806–812, https://doi.org/10.1038/s41566-017-0049-4.
- [26] S. Tan, L. Liu, Y. Dai, J. Ren, J. Zhao, H. Petek, Ultrafast plasmon-enhanced hot electron generation at Ag nanocluster/graphite heterojunctions, J. Am. Chem. Soc. 139 (17) (2017) 6160–6168, https://doi.org/10.1021/jacs.7b01079.
- [27] S. Tan, Y. Dai, S. Zhang, L. Liu, J. Zhao, H. Petek, Coherent electron transfer at the Ag/graphite heterojunction interface, Phys. Rev. Lett. 120 (2018), 126801. https://journals.aps.org/prl/abstract/10.1103/PhysRevLett.120.126801.
- [28] W.S. Fann, R. Storz, H.W.K. Tom, J. Bokor, Electron thermalization in gold, Phys. Rev. B 46 (1992), 13592. http://link.aps.org/doi/10.1103/PhysRevB.46.
- [29] C.A. Schmuttenmaer, M. Aeschlimann, H.E. Elsayed-Ali, R.J.D. Miller, D.A. Mantell, J. Cao, Y. Gao, Time-resolved two-photon photoemission from Cu(100): energy dependence of electron relaxation, Phys. Rev. B 50 (1994), 8957. http://link.aps.org/doi/10.1103/PhysRevB.50.8957.
- [30] E. Knoesel, T. Hertel, M. Wolf, G. Ertl, Femtosecond dynamics of electronic excitations of adsorbates studied by two-photon photoemission pulse correlation: CO/Cu(111), Chem. Phys. Lett. 240 (1995), 409. http://www.sciencedirect.com/science/article/B6TFN-3YCN3GW-FF/2/bef32e956ff95b054b488a5c403b303a.
- [31] M. Aeschlimann, S. Pawlik, M. Bauer, Femtosecond time-resolved measurement of electron relaxation at metal surfaces, Ber. Bunsen Ges. 99 (12) (1995) 1504–1508
- [32] S. Ogawa, H. Petek, Femtosecond dynamics of hot-electron relaxation in Cu(110) and Cu(100), Surf. Sci. 357–358 (1996), 585. http://www.sciencedirect.com/science/article/B6TVX-3YF4R4N-82/2/6bf3a1aa1752388af63dd6be57721d07.
- [33] T. Hertel, E. Knoesel, M. Wolf, G. Ertl, Ultrafast electron dynamics at Cu(111): response of an electron gas to optical excitation, Phys. Rev. Lett. 76 (1996), 535. http://link.aps.org/doi/10.1103/PhysRevLett.76.535.
- [34] S. Ogawa, H. Nagano, H. Petek, Hot-electron dynamics at Cu(100), Cu(110) and Cu(111) surfaces: comparison of experiment with Fermi liquid theory, Phys. Rev. B 55 (1997), 10869. http://prb.aps.org/abstract/PRB/v55/i16/p10869_1.
- [35] W. Nessler, S. Ogawa, H. Nagano, H. Petek, J. Shimoyama, Y. Nakayama, K. Kishio, Femtosecond time-resolved study of the energy and temperature dependence of hot-electron lifetimes in Bi₂Sr₂CaCu₂O_{8+δt} Phys. Rev. Lett. 81 (1998), 4480. http://link.aps.org/doi/10.1103/PhysRevLett.81.4480.
- [36] H. Petek, H. Nagano, M.J. Weida, S. Ogawa, The role of auger decay in hot electron excitation in copper, Chem. Phys. 251 (2000), 71. https://www.sciencedirect.com/science/article/pii/S0301010499003031
- [37] M.J. Weida, S. Ogawa, H. Nagano, H. Petek, Parallel excitation pathways in ultrafast interferometric pump-probe correlation measurements of hot-electron lifetimes in metals, Appl. Phys. A 71 (5) (2000) 553–559, https://doi.org/10.1007/s003390000713.
- [38] M. Bauer, A. Marienfeld, M. Aeschlimann, Hot electron lifetimes in metals probed by time-resolved two-photon photoemission, Prog. Surf. Sci. 90 (2015), 319. http://www.sciencedirect.com/science/article/pii/S0079681615000192.
- [39] M. Reutzel, A. Li, H. Petek, Coherent two-dimensional multiphoton photoelectron spectroscopy of metal surfaces, Phys. Rev. X 9 (2019), 011044. https://link.aps.org/doi/10.1103/PhysRevX.9.011044.
- [40] M. Reutzel, A. Li, H. Petek, Above-threshold multiphoton photoemission from noble metal surfaces, Phys. Rev. B 101 (2020), 075409. https://link.aps.org/doi/10.1103/PhysRevB.101.075409.
- [41] M. Reutzel, A. Li, B. Gumhalter, H. Petek, Nonlinear plasmonic photoelectron response of Ag(111), Phys. Rev. Lett. 123 (2019), 017404. https://link.aps.org/doi/10.1103/PhysRevLett.123.017404.
- [42] A. Li, N.A. James, T. Wang, Z. Wang, H. Petek, M. Reutzel, Towards full surface Brillouin zone mapping by coherent multi-photon photoemission, New J. Phys. 22 (7) (2020), https://doi.org/10.1088/1367-2630/ab98d6.
- [43] A. Li, M. Reutzel, Z. Wang, D. Novko, B. Gumhalter, H. Petek, Plasmonic photoemission from single-crystalline silver, ACS Photon. 8 (1) (2021) 247–258, https://doi.org/10.1021/acsphotonics.0c01412.
- [44] D. Novko, V. Despoja, M. Reutzel, A. Li, H. Petek, B. Gumhalter, Plasmonically assisted channels of photoemission from metals, Phys. Rev. B 103 (2021), 205401, https://doi.org/10.1103/PhysRevB.103.205401.
- [45] A. Li, et al., Multidimensional multiphoton momentum microscopy of the anisotropic Ag(110) surface, Phys. Rev. B 105 (2022), 075105, https://doi.org/10.1103/PhysRevB.105.075105.
- [46] B. Gumhalter, D. Novko, H. Petek, Electron emission from plasmonically induced floquet bands at metal surfaces, Phys. Rev. B 106 (2022), 035422. https://link.aps.org/doi/10.1103/PhysRevB.106.035422.
- [47] N.V. Smith, W.E. Spicer, Photoemission studies of the alkali metals. I. Sodium and Potassium, Phys. Rev. 188 (1969), 593, https://doi.org/10.1103/ PhysRev.188.593.

- [48] N.V. Smith, G.B. Fisher, Photoemission studies of the alkali metals. II Rubidium and Cesium, Phys. Rev. B 3 (1971), 3662, https://doi.org/10.1103/
- [49] J.J. Hopfield, Effect of electron-electron interactions on photoemission in simple metals, Phys. Rev. 139 (1965), A419, https://doi.org/10.1103/PhysRev.139.
- [50] S.R. Barman, C. Biswas, K. Horn, Electronic excitations on silver surfaces, Phys. Rev. B 69 (2004), 045413, https://doi.org/10.1103/PhysRevB.69.045413.
- [51] S.R. Barman, C. Biswas, K. Horn, Collective excitations on silver surfaces studied by photoyield, Surf. Sci. 566–568, Part 1 (2004), 538. http://www.sciencedirect.com/science/article/pii/S0039602804007241.
- [52] B. Gumhalter, D. Novko, Complementary perturbative and nonperturbative pictures of plasmonically induced electron emission from flat metal surfaces, Progress in Surface Science, The following article, 2023.
- [53] K. Kempa, F. Forstmann, The electromagnetic field and the photoyield at metal surfaces from the hydrodynamic approximation, Surf. Sci. 129 (1983), 516. https://www.sciencedirect.com/science/article/pii/0039602883901954.
- [54] P. Apell, Å. Ljungbert, S. Lundqvist, Non-local optical effects at metal surfaces, Phys. Scr. 30 (1984), 367. http://stacks.iop.org/1402-4896/30/i=5/a=014.
- [55] Y. Wang, E.W. Plummer, K. Kempa, Foundations of plasmonics, Adv. Phys. 60 (5) (2011) 799-898, https://doi.org/10.1080/00018732.2011.621320.
- [56] S.R. Barman, K. Horn, P. Häberle, H. Ishida, A. Liebsch, Photoinduced plasmon excitations in alkali-metal overlayers, Phys. Rev. B 57 (1998), 6662. http://link.aps.org/doi/10.1103/PhysRevB.57.6662.
- [57] E.E. Krasovskii, V.M. Silkin, V.U. Nazarov, P.M. Echenique, E.V. Chulkov, Dielectric screening and band-structure effects in low-energy photoemission, Phys. Rev. B 82 (2010), 125102, https://doi.org/10.1103/PhysRevB.82.125102.
- [58] S. Tanaka, T. Yoshida, K. Watanabe, Y. Matsumoto, T. Yasuike, M. Petrović, M. Kralj, Linewidth narrowing with ultimate confinement of an alkali multipole plasmon by modifying surface electronic wave functions with two-dimensional materials, Phys. Rev. Lett. 125 (2020), 126802, https://doi.org/10.1103/PhysRevLett.125.126802.
- [59] A. Marini, R. Del Sole, G. Onida, First-principles calculation of the plasmon resonance and of the reflectance spectrum of silver in the GW approximation, Phys. Rev. B 66 (2002), 115101. http://link.aps.org/abstract/PRB/v66/e115101.
- [60] A. Rodríguez Echarri, P.A.D. Gonçalves, C. Tserkezis, F.J. García de Abajo, N.A. Mortensen, J.D. Cox, Optical response of noble metal nanostructures: quantum surface effects in crystallographic facets, Optica 8 (2021), 710. http://opg.optica.org/optica/abstract.cfm?URI=optica-8-5-710.
- [61] M. Paleschke, C.-T. Chiang, L. Brandt, N. Liebing, G. Woltersdorf, W. Widdra, Plasmonic spin-hall effect of propagating surface plasmon polaritons in Ni₈₀Fe₂₀ microstructures, New J. Phys. 23 (9) (2021), 093006, https://doi.org/10.1088/1367-2630/ac1c83.
- [62] P. Nozières, D. Pines, Electron interaction in solids. General formulation, Phys. Rev. 109 (1958), 741, https://doi.org/10.1103/PhysRev.109.741.
- [63] A. Liebsch, Dynamical screening at simple-metal surfaces, Phys. Rev. B 36 (14) (1987) 7378-7388.
- [64] J.A. Dionne, Mirror, Mirror, Physics 38 (2012) 7378-7388. URL: http://link.aps.org/doi/10.1103/Physics.5.38.
- [65] M.Z. Alam, I.D. Leon, R.W. Boyd, Large optical nonlinearity of indium tin oxide in its epsilon-near-zero region, Science 352 (2016), 795. https://science.sciencemag.org/content/352/6287/795.
- [66] O. Reshef, E. Giese, M. Zahirul Alam, I. De Leon, J. Upham, R.W. Boyd, Beyond the perturbative description of the nonlinear optical response of low-index materials, Opt. Lett. 42 (2017), 3225. https://www.ncbi.nlm.nih.gov/pubmed/28809914.
- [67] O. Reshef, I. De Leon, M.Z. Alam, R.W. Boyd, Nonlinear optical effects in epsilon-near-zero media, Nat. Rev. Mater. 4 (2019), 535, https://doi.org/10.1038/e41578.019.0120.5
- [68] I. Liberal, N. Engheta, How does light behave in a material whose refractive index vanishes? Phys. Today 75 (2022), 62. https://physicstoday.scitation.org/doi/abs/10.1063/PT.3.4968.
- [69] N.B. Grosse, J. Heckmann, U. Woggon, Nonlinear plasmon-photon interaction resolved by k-space spectroscopy, Phys. Rev. Lett. 108 (2012), 136802, https://doi.org/10.1103/PhysRevLett.108.136802.
- [70] H.J. Levinson, E.W. Plummer, The surface photoeffect, Phys. Rev. B 24 (1981), 628. http://link.aps.org/abstract/PRB/v24/p628.
- [71] P.J. Feibelman, Surface electromagnetic fields, Prog. Surf. Sci. 12 (1982), 287. https://www.sciencedirect.com/science/article/pii/0079681682900016.
- [72] K. Kempa, W.L. Schaich, Nonlocal corrections to Fresnel optics: Jellium-model calculations above the bulk-plasmon threshold, Physical Review B 39 (1989), 13139. https://link.aps.org/doi/10.1103/PhysRevB.39.13139.
- [73] A. Liebsch, W.L. Schaich, Influence of a polarizable medium on the nonlocal optical response of a metal surface, Phys. Rev. B 52 (1995), 14219. http://link.aps.org/doi/10.1103/PhysRevB.52.14219.
- [74] A. Kubo, Y.S. Jung, H.K. Kim, H. Petek, Femtosecond microscopy of localized and propagating surface plasmons in silver gratings, J. Phys. B Atomic Mol. Phys. 40 (2007), S259. http://stacks.iop.org/0953-4075/40/S259.
- [75] A. Kubo, N. Pontius, H. Petek, Femtosecond microscopy of surface plasmon polariton wave packet evolution at the silver/vacuum interface, Nano Lett. 7 (2007), 470. http://pubs.acs.org/doi/abs/10.1021/nl0627846?prevSearch=%255BContrib%253A%2Bpetek%255D&searchHistoryKey=.
- [76] J.J. Hopfield, Theory of the contribution of excitons to the complex dielectric constant of crystals, Phys. Rev. 112 (1958), 1555. http://link.aps.org/doi/10. 1103/PhysRev.112.1555.
- [77] S. Link, M.A. El-Sayed, Size and temperature dependence of the plasmon absorption of colloidal gold nanoparticles, J. Phys. Chem. B 103 (21) (1999) 4212–4217, https://doi.org/10.1021/jp9847960.
- [78] M. Zhou, X. Du, H.e. Wang, R. Jin, The critical number of gold atoms for a metallic state nanocluster: resolving a decades-long question, ACS Nano 15 (9) (2021) 13980–13992, https://doi.org/10.1021/acsnano.1c04705.
- [79] R. Zhang, Y. Zhang, Z.C. Dong, S. Jiang, C. Zhang, L.G. Chen, L. Zhang, Y. Liao, J. Aizpurua, Y. Luo, J.L. Yang, J.G. Hou, Chemical mapping of a single molecule by plasmon-enhanced Raman scattering, Nature 498 (7452) (2013) 82–86, https://doi.org/10.1038/nature12151.
- [80] S. Yampolsky, D.A. Fishman, S. Dey, E. Hulkko, M. Banik, E.O. Potma, V.A. Apkarian, Seeing a single molecule vibrate through time-resolved coherent anti-Stokes Raman scattering, Nat. Photonics 8 (8) (2014) 650–656, https://doi.org/10.1038/nphoton.2014.143.
- [81] M. Banik, K. Rodriguez, E. Hulkko, V.A. Apkarian, Orientation-dependent handedness of chiral plasmons on nanosphere dimers: how to turn a right hand into a left hand, ACS Photonics 3 (12) (2016) 2482–2489, https://doi.org/10.1021/acsphotonics.6b00733.
- [82] S. Li, S. Chen, J. Li, R. Wu, W. Ho, Joint space-time coherent vibration driven conformational transitions in a single molecule, Phys. Rev. Lett. 119 (2017), 176002. https://link.aps.org/doi/10.1103/PhysRevLett.119.176002.
- [83] L. Bi, K. Liang, G. Czap, H. Wang, K. Yang, S. Li, Recent progress in probing atomic and molecular quantum coherence with scanning tunneling microscopy, Prog. Surf. Sci. (2022), 100696. https://www.sciencedirect.com/science/article/pii/S0079681622000442.
- [84] J. Lee, K.T. Crampton, N. Tallarida, V.A. Apkarian, Visualizing vibrational normal modes of a single molecule with atomically confined light, Nature 568 (7750) (2019) 78–82, https://doi.org/10.1038/s41586-019-1059-9.
- [85] S. Lu, L. Xie, K. Lai, R. Chen, L.u. Cao, K. Hu, X. Wang, J. Han, X. Wan, J. Wan, Q. Dai, F. Song, J. He, J. Dai, J. Chen, Z. Wang, G. Wang, Plasmonic evolution of atomically size-selected Au clusters by electron energy loss spectrum, Natl. Sci. Rev. 8 (12) (2021), https://doi.org/10.1093/nsr/nwaa282.
- [86] G.W. Bryant, F.J. García de Abajo, J. Aizpurua, Mapping the plasmon resonances of metallic nanoantennas, Nano Lett. 8 (2) (2008) 631–636, https://doi.org/10.1021/nl073042v.
- [87] T.H. Taminiau, F.D. Stefani, N.F. van Hulst, Optical nanorod antennas modeled as cavities for dipolar emitters: evolution of sub- and super-radiant modes, Nano Lett. 11 (3) (2011) 1020–1024, https://doi.org/10.1021/nl103828n.
- [88] J. Pettine, D.J. Nesbitt, Emerging methods for controlling hot carrier excitation and emission distributions in nanoplasmonic systems, J. Phys. Chem. C 126 (35) (2022) 14767–14780, https://doi.org/10.1021/acs.jpcc.2c03425.
- [89] H. Ditlbacher, A. Hohenau, D. Wagner, U. Kreibig, M. Rogers, F. Hofer, F.R. Aussenegg, J.R. Krenn, Silver nanowires as surface plasmon resonators, Phys. Rev. Lett. 95 (2005), 257403. http://link.aps.org/abstract/PRL/v95/e257403.
- [90] D. Rossouw, M. Couillard, J. Vickery, E. Kumacheva, G.A. Botton, Multipolar plasmonic resonances in silver nanowire antennas imaged with a subnanometer electron probe, Nano Lett. 11 (4) (2011) 1499–1504, https://doi.org/10.1021/nl200634w.

- [91] L. Piazza, T.T.A. Lummen, E. Quiñonez, Y. Murooka, B.W. Reed, B. Barwick, F. Carbone, Simultaneous observation of the quantization and the interference pattern of a plasmonic near-field, Nat. Commun. 6 (2015), 6407, https://doi.org/10.1038/ncomms7407.
- [92] Y. Wu, Z. Hu, X.-T. Kong, J.C. Idrobo, A.G. Nixon, P.D. Rack, D.J. Masiello, J.P. Camden, Infrared plasmonics: STEM-EELS characterization of Fabry-Pérot resonance damping in gold nanowires, Phys. Rev. B 101 (2020), 085409, https://doi.org/10.1103/PhysRevB.101.085409.
- [93] M. Dabrowski, Y. Dai, A. Argondizzo, Q. Zou, X. Cui, H. Petek, Multiphoton photoemission microscopy of high-order plasmonic resonances at the Ag/Vacuum and Ag/Si interfaces of epitaxial silver nanowires, ACS Photonics 3 (2016) 1704–1713, https://doi.org/10.1021/acsphotonics.6b00353.
- [94] L.I. Chelaru, F.-J. Meyer zu Heringdorf, In situ monitoring of surface plasmons in single-crystalline Ag-nanowires, Surf. Sci. 601 (2007), 4541. http://www.sciencedirect.com/science/article/pii/S0039602807004748.
- [95] A. Losquin, T.T.A. Lummen, Electron microscopy methods for space-, energy-, and time-resolved plasmonics, Front. Phys. 12 (2016), 127301, https://doi.org/10.1007/s11467-016-0605-2
- [96] O. Nicoletti, M. Wubs, N.A. Mortensen, W. Sigle, P.A. van Aken, P.A. Midgley, Surface plasmon modes of a single silver nanorod: an electron energy loss study, Opt. Express 19 (2011), 15371. http://www.opticsexpress.org/abstract.cfm?URI=oe-19-16-15371.
- [97] C. Hogan, O. Pulci, P. Gori, F. Bechstedt, D.S. Martin, E.E. Barritt, A. Curcella, G. Prevot, Y. Borensztein, Optical properties of silicene, Si/Ag(111), and Si/Ag (110), Phys. Rev. B 97 (2018), 195407. https://link.aps.org/doi/10.1103/PhysRevB.97.195407.
- [98] P. Berini, Long-range surface plasmon polaritons, Adv. Opt. Photon. 1 (2009), 484. http://aop.osa.org/abstract.cfm?URI=aop-1-3-484.
- [99] M. Rocca, Low-energy EELS investigation of surface electronic excitations on metals, Surf. Sci. Rep. 22 (1995), 1. https://www.sciencedirect.com/science/article/pii/0167572995000046.
- [100] K.Y. Bliokh, F.J. Rodríguez-Fortuño, F. Nori, A.V. Zayats, Spin-orbit interactions of light, Nat Photon 9 (12) (2015) 796–808, https://doi.org/10.1038/nphoton.2015.201.
- [101] K.Y. Bliokh, D. Leykam, M. Lein, F. Nori, Topological non-hermitian origin of surface maxwell waves, Nat. Commun. 10 (2019), 580, https://doi.org/10.1038/s41467-019-08397-6.
- [102] T. Van Mechelen, Z. Jacob, Nonlocal topological electromagnetic phases of matter, Phys. Rev. B 99 (2019), 205146. https://link.aps.org/doi/10.1103/ PhysRevB.99.205146.
- [103] Y. Dai, Z. Zhou, A. Ghosh, R.S.K. Mong, A. Kubo, C.-B. Huang, H. Petek, Plasmonic topological quasiparticle on the nanometre and femtosecond scales, Nature 588 (2020), 616. https://www.nature.com/articles/s41586-020-3030-1.
- [104] Y. Dai, Z. Zhou, A. Ghosh, S. Yang, C.-B. Huang, H. Petek, Ultrafast nanofemto photoemission electron microscopy of vectorial plasmonic fields, MRS Bull. 46 (8) (2021) 738–746, https://doi.org/10.1557/s43577-021-00152-x.
- [105] A. Ghosh, S. Yang, Y. Dai, Z. Zhou, T. Wang, C.-B. Huang, H. Petek, A topological lattice of plasmonic merons, Appl. Phys. Rev. 8 (2021), 041413. https://aip.scitation.org/doi/abs/10.1063/5.0062133.
- [106] Y. Dai, A. Ghosh, S. Yang, Z. Zhou, C.-B. Huang, H. Petek, Poincaré engineering of surface plasmon polaritons, Nat. Rev. Phys. 4 (9) (2022) 562–564, https://doi.org/10.1038/s42254-022-0049-w
- [107] Y. Dai, Z. Zhou, A. Ghosh, K. Kapoor, M. Dabrowski, A. Kubo, C.-B. Huang, H. Petek, Ultrafast microscopy of a twisted plasmonic spin skyrmion, Appl. Phys. Rev. 9 (2022), 011420. https://aip.scitation.org/doi/abs/10.1063/5.0084482.
- [108] A. Ghosh, S. Yang, Y. Dai, H. Petek, The spin texture topology of polygonal plasmon fields, ACS Photonics 10 (1) (2023) 13–23, https://doi.org/10.1021/acsphotonics.2c01491.
- [109] K.Y. Bliokh, F. Nori, Transverse spin of a surface polariton, Phys. Rev. A 85 (2012), 061801, https://doi.org/10.1103/PhysRevA.85.061801.
- [110] K.Y. Bliokh, F. Nori, Transverse and longitudinal angular momenta of light, Phys. Rep. 592 (2015), 1. http://www.sciencedirect.com/science/article/pii/ S0370157315003336
- [111] T. Van Mechelen, Z. Jacob, Universal spin-momentum locking of evanescent waves, Optica 3 (2) (2016), 118.
- [112] K.Y. Bliokh, D. Smirnova, F. Nori, Quantum spin hall effect of light, Science 348 (2015), 1448. http://science.sciencemag.org/content/348/6242/1448.
- [113] A. Aiello, P. Banzer, M. Neugebauer, G. Leuchs, From transverse angular momentum to photonic wheels, Nat. Photon. 9 (12) (2015) 789–795, https://doi.org/
- [114] A. Aiello, P. Banzer, The ubiquitous photonic wheel, J. Opt. 18 (2016), 085605, https://doi.org/10.1088/2040-8978/18/8/085605.
- [115] B.-Y. Xie, H.-F. Wang, X.-Y. Zhu, M.-H. Lu, Z.D. Wang, Y.-F. Chen, Photonics meets topology, Opt. Express 26 (2018), 24531. http://www.opticsexpress.org/abstract.cfm?URI=oe-26-19-24531.
- [116] L. Du, A. Yang, A.V. Zayats, X. Yuan, Deep-subwavelength features of photonic skyrmions in a confined electromagnetic field with orbital angular momentum, Nat. Phys. 15 (7) (2019) 650–654, https://doi.org/10.1038/s41567-019-0487-7.
- [117] P. Shi, L. Du, X. Yuan, Spin photonics: from transverse spin to photonic skyrmions, Nanophotonics 10 (2021), 3927, https://doi.org/10.1515/nanoph-2021-0046.
- [118] M.S. Rider, Á. Buendía, D.R. Abujetas, P.A. Huidobro, J.A. Sánchez-Gil, V. Giannini, Advances and prospects in topological nanoparticle photonics, ACS Photonics 9 (5) (2022) 1483–1499, https://doi.org/10.1021/acsphotonics.1c01874.
- [119] Y. Bai, J. Yan, H. Lv, Y. Yang, Plasmonic vortices: a review, J. Opt. 24 (2022), 084004, https://doi.org/10.1088/2040-8986/ac7d5f.
- [120] K.Y. Bliokh, et al., Roadmap on structured waves, J. Opt. (2023).
- [121] M. Rocca, in: Springer handbook of surface science, Springer International Publishing, Cham, 2020, 531.
- [122] M.A. Cazalilla, J.S. Dolado, A. Rubio, P.M. Echenique, Plasmonic excitations in noble metals: the case of Ag, Phys. Rev. B 61 (2000), 8033. http://link.aps.org/abstract/PRB/v61/p8033.
- [123] L. Calmels, J.E. Inglesfield, E. Arola, S. Crampin, T. Rasing, Local-field effects on the near-surface and near-interface screened electric field in noble metals, Phys. Rev. B 64 (2001), 125416, https://doi.org/10.1103/PhysRevB.64.125416.
- [124] L. Zhang, A. Kubo, L. Wang, H. Petek, T. Seideman, Imaging of surface plasmon polariton fields excited at a nanometer-scale slit, Phys. Rev. B 84 (2011), 245442. https://doi.org/10.1103/PhysRevB.84.245442.
- [125] L. Zhang, A. Kubo, L. Wang, H. Petek, T. Seideman, Universal aspects of ultrafast optical pulse scattering by a nanoscale asperity, J. Phys. Chem. C 117 (36) (2013) 18648–18652, https://doi.org/10.1021/jp4076614.
- [126] L.-M. Wang, L. Zhang, T. Seideman, H. Petek, Dynamics of coupled plasmon polariton wave packets excited at a subwavelength slit in optically thin metal films. Phys. Rev. B 86 (2012), 165408. http://link.aps.org/doi/10.1103/PhysRevB.86.165408.
- [127] L.-M. Wang, H. Petek, Focusing surface plasmon polariton wave packets in space and time, Laser Photonics Rev. 7 (6) (2013) 1003–1009, https://doi.org/
- [128] D. Podbiel, P. Kahl, A. Makris, B. Frank, S. Sindermann, T.J. Davis, H. Giessen, M. Horn-von, Hoegen, F.-J. Meyer, zu, Heringdorf, Imaging the nonlinear plasmoemission dynamics of electrons from strong plasmonic fields, Nano Lett. 17 (2017), 6569. https://www.ncbi.nlm.nih.gov/pubmed/28945435.
- [129] G. Spektor, D. Kilbane, A.K. Mahro, M. Hartelt, E. Prinz, M. Aeschlimann, M. Orenstein, Mixing the light spin with plasmon orbit by nonlinear light-matter interaction in gold, Phys. Rev. X 9 (2019), 021031, https://doi.org/10.1103/PhysRevX.9.021031.
- [130] T.J. Davis, D. Janoschka, P. Dreher, B. Frank, F.-J. Meyer zu Heringdorf, H. Giessen, Ultrafast vector imaging of plasmonic skyrmion dynamics with deep subwavelength resolution, Science 368 (2020), eaba6415.
- [131] R. Ron, T. Zar, A. Salomon, Linear and nonlinear optical properties of well-defined and disordered plasmonic systems: a review, Adv. Opt. Mater. 11 (2023), 2201475. https://doi.org/10.1002/adom.202201475.
- [132] A. Otto, Excitation of nonradiative surface plasma waves in silver by the method of frustrated total reflection, Zeitschrift für Physik A Hadrons nuclei 216 (4) (1968) 398–410. https://doi.org/10.1007/BF01391532.
- [133] E. Kretschmann, Decay of non radiative surface plasmons into light on rough silver films. Comparison of experimental and theoretical results, Opt. Commun. 6 (1972), 185. http://www.sciencedirect.com/science/article/pii/0030401872902246.

- [134] Y. Dai, H. Petek, Plasmonic spin-hall effect in surface plasmon polariton focusing, ACS Photon. 6 (8) (2019) 2005–2013, https://doi.org/10.1021/
- [135] Y. Dai, M. Dabrowski, H. Petek, Optical field tuning of localized plasmon modes in Ag microcrystals at the nanofemto scale, J. Chem. Phys. 152 (2020), 054201, https://doi.org/10.1063/1.5139543.
- [136] M. Dabrowski, Y. Dai, H. Petek, Ultrafast photoemission electron microscopy: imaging plasmons in space and time, Chem. Rev. 120 (13) (2020) 6247–6287, https://doi.org/10.1021/acs.chemrev.0c00146.
- [137] Y. Dai, M. Dabrowski, V.A. Apkarian, H. Petek, Ultrafast microscopy of spin-momentum-locked surface plasmon polaritons, ACS Nano 12 (2018), 6588, https://doi.org/10.1021/acsnano.8b01386.
- [138] M. Aeschlimann, et al., Coherent two-dmensional nanoscopy, Science 333 (2011), 1723. http://www.sciencemag.org/content/333/6050/1723.abstract.
- [139] M. Dąbrowski, Y. Dai, H. Petek, Ultrafast microscopy: imaging light with photoelectrons on the nano-femto scale, J. Phys. Chem. Lett. 8 (18) (2017) 4446–4455, https://doi.org/10.1021/acs.jpclett.7b00904.
- [140] P. Kahl, D. Podbiel, C. Schneider, A. Makris, S. Sindermann, C. Witt, D. Kilbane, M.-V. Hoegen, M. Aeschlimann, F.M. zu Heringdorf, Direct observation of surface plasmon polariton propagation and interference by time-resolved imaging in normal-incidence two photon photoemission microscopy, Plasmonics 13 (1) (2018) 239–246, https://doi.org/10.1007/s11468-017-0504-6.
- [141] B. Frank, et al., Short-range surface plasmonics: localized electron emission dynamics from a 60-nm spot on an atomically flat single-crystalline gold surface, Sci. Adv. 3 (2017), e1700721. http://advances.sciencemag.org/content/advances/3/7/e1700721.full.pdf.
- [142] N. Ichiji, H. Kikuchi, M. Yessenov, K.L. Schepler, A.F. Abouraddy, A. Kubo, Observation of ultrabroadband striped space-time surface plasmon polaritons, ACS Photonics 10 (2) (2023) 374–382, https://doi.org/10.1021/acsphotonics.2c00296.
- [143] G. Spektor, et al., Revealing the subfemtosecond dynamics of orbital angular momentum in nanoplasmonic vortices, Science 355 (2017), 1187. http://science.sciencemag.org/content/sci/355/6330/1187.full.pdf.
- [144] F.J. Rodríguez-Fortuño, G. Marino, P. Ginzburg, D. O'Connor, A. Martínez, G.A. Wurtz, A.V. Zayats, Near-Field interference for the unidirectional excitation of electromagnetic guided modes, Science 340 (2013), 328. http://science.sciencemag.org/content/sci/340/6130/328.full.pdf.
- [145] K.D. Tsuei, E.W. Plummer, A. Liebsch, E. Pehlke, K. Kempa, P. Bakshi, The normal modes at the surface of simple metals, Surf. Sci. 247 (1991), 302. http://www.sciencedirect.com/science/article/pii/003960289190142F.
- [146] Y. Borensztein, W.L. Mochan, J. Tarriba, R.G. Barrera, A. Tadjeddine, Large anisotropy in the optical reflectance of Ag(110) single crystals: experiment and theory, Phys. Rev. Lett. 71 (1993), 2334. https://link.aps.org/doi/10.1103/PhysRevLett.71.2334.
- [147] C. Schwartz, W.L. Schaich, Multipole surface plasmons and photoemission yield spectra, Phys. Rev. B 30 (2) (1984) 1059-1061.
- [148] S.R. Barman, K. Horn, Photoemission study of electronic excitations at clean metal surfaces and thin metal films, Appl. Phys. A 69 (5) (1999) 519–527, https://doi.org/10.1007/s003390051458.
- [149] F. Moresco, M. Rocca, V. Zielasek, T. Hildebrandt, M. Henzler, Evidence for the presence of the multipole plasmon mode on Ag surfaces, Phys. Rev. B 54 (1996), R14333, https://doi.org/10.1103/PhysRevB.54.R14333.
- [150] J.J. Quinn, Multipole plasmon modes at the surface of a conducting solid, Solid State Commun. 84 (1992), 139. https://www.sciencedirect.com/science/article/pii/003810989290311V.
- [151] M. Merschdorf, C. Kennerknecht, W. Pfeiffer, Collective and single-particle dynamics in time-resolved two-photon photoemission, Phys. Rev. B 70 (2004), 193401. http://link.aps.org/abstract/PRB/v70/e193401.
- [152] G. Raseev, Plasmon resonances of Ag(001) and Ag(111) studied by power density absorption and photoyield, Surf. Sci. 615 (2013), 6. http://www.sciencedirect.com/science/article/pii/S0039602813000563.
- [153] J.B. Khurgin, Hot carriers generated by plasmons: where are they generated and where do they go from there? Faraday Discuss. 214 (2019), 35 https://doi.org/10.1039/C8FD00200B.
- [154] J.B. Khurgin, Fundamental limits of hot carrier injection from metal in nanoplasmonics, Nanophotonics 9 (2020), 453, https://doi.org/10.1515/nanoph-2019-0206
- [155] R. L. Gieseking, M. A. Ratner, and G. C. Schatz, in Frontiers of Plasmon Enhanced Spectroscopy Volume 1 (American Chemical Society, 2016), pp. 1.
- [156] P. Nozières, D. Pines, Electron interaction in solids. Characteristic energy loss spectrum, Phys. Rev. 113 (1959), 1254, https://doi.org/10.1103/
- [157] S. Ogawa, H. Nagano, H. Petek, A.P. Heberle, Optical dephasing in Cu(111) measured by interferometric two-photon time-resolved photoemission, Phys. Rev. Lett. 78 (1997), 1339. http://prl.aps.org/abstract/PRL/v78/i7/p1339_1.
- [158] H. Petek, A.P. Heberle, W. Nessler, H. Nagano, S. Kubota, S. Matsunami, N. Moriya, S. Ogawa, Optical phase control of coherent electron dynamics in metals, Phys. Rev. Lett. 79 (1997), 4649. http://prl.aps.org/abstract/PRL/v79/i23/p4649 1.
- [159] H. Petek, H. Nagano, S. Ogawa, Hole decoherence of d bands in copper, Phys. Rev. Lett. 83 (1999), 832, https://doi.org/10.1103/PhysRevLett.83.832.
- [160] A. Kubo, K. Onda, H. Petek, Z. Sun, Y.S. Jung, H.K. Kim, Femtosecond imaging of surface plasmon dynamics in a nanostructured silver film, Nano Lett. 5 (6) (2005) 1123–1127, https://doi.org/10.1021/nl0506655.
- [161] A. Winkelmann, W.-C. Lin, F. Bisio, H. Petek, J. Kirschner, Interferometric control of spin-polarized electron populations at a metal surface observed by multiphoton photoemission, Phys. Rev. Lett. 100 (2008), 206601. http://link.aps.org/abstract/PRL/v100/e206601.
- [162] M. Reutzel, A. Li, Z. Wang, H. Petek, Coherent multidimensional photoelectron spectroscopy of ultrafast quasiparticle dressing by light, Nature Commun. 11 (2020), 2230, https://doi.org/10.1038/s41467-020-16064-4.
- [163] H. Petek, H. Nagano, S. Ogawa, Hot-electron dynamics in copper revisited: the d-band effect, Appl. Phys. B 68 (3) (1999) 369–375, https://doi.org/10.1007/s003400050634.
- [164] V. Halté, J. Guille, J.C. Merle, I. Perakis, J.Y. Bigot, Electron dynamics in silver nanoparticles: comparison between thin films and glass embedded nanoparticles, Phys. Rev. B 60 (1999), 11738, https://doi.org/10.1103/PhysRevB.60.11738.
- [165] I.E. Perakis, T.V. Shahbazyan, Many-body correlation effects in the ultrafast non-linear optical response of confined Fermi seas, Surf. Sci. Rep. 40 (2000), 1. http://www.sciencedirect.com/science/article/pii/S0167572900000091.
- [166] N. Del Fatti, C. Voisin, M. Achermann, S. Tzortzakis, D. Christofilos, F. Vallée, Nonequilibrium electron dynamics in noble metals, Phys. Rev. B 61 (2000), 16956, https://doi.org/10.1103/PhysRevB.61.16956.
- [167] M. Pelton, J. Aizpurua, G. Bryant, Metal-nanoparticle plasmonics, Laser & Photon. Rev. 2 (3) (2008) 136–159, https://doi.org/10.1002/lpor.200810003.
- [168] F. Bisio, A. Winkelmann, W.C. Lin, C.T. Chiang, M. Nývlt, H. Petek, J. Kirschner, Band structure effects in surface second harmonic generation: the case of Cu (001), Phys. Rev. B 80 (2009), 125432. http://link.aps.org/abstract/PRB/v80/e125432.
- [169] T. Haug, P. Klemm, S. Bange, J.M. Lupton, Hot-electron intraband luminescence from single hot spots in noble-metal nanoparticle films, Phys. Rev. Lett. 115 (2015), 067403, https://doi.org/10.1103/PhysRevLett.115.067403.
- [170] M. Pelton, Modified spontaneous emission in nanophotonic structures, Nat. Photon. 9 (7) (2015) 427-435, https://doi.org/10.1038/nphoton.2015.103.
- [171] F. Bisio, M. Nývlt, J. Franta, H. Petek, J. Kirschner, Mechanisms of high-order perturbative photoemission from Cu(001), Phys. Rev. Lett. 96 (2006), 087601. http://link.aps.org/doi/10.1103/PhysRevLett.96.087601.
- [172] L. Brus, Noble metal nanocrystals: plasmon electron transfer photochemistry and single-molecule Raman spectroscopy, Acc. Chem. Res. 41 (12) (2008) 1742–1749, https://doi.org/10.1021/ar800121r.
- [173] K.L. Kliewer, K.H. Bennemann, Photoemission from the Drude absorption, Phys. Rev. B 15 (1977), 3731, https://doi.org/10.1103/PhysRevB.15.3731.
- [174] H.U. Yang, J. D'Archangel, M.L. Sundheimer, E. Tucker, G.D. Boreman, M.B. Raschke, Optical dielectric function of silver, Phys. Rev. B 91 (2015), 235137, https://doi.org/10.1103/PhysRevB.91.235137.
- [175] N. W. Ashcroft and N. D. Mermin, Solid State Physics (Brooks/Cole, Belmont, 1976), pp. 826.
- [176] C. López-Bastidas, W.L. Mochán, Local field effects in the dynamical response of Ag, Phys. Status Solidi (a) 170 (1998), 323. https://onlinelibrary.wiley.com/doi/abs/10.1002/%28SICI%291521-396X%28199812%29170%3A2%3C323%3A%3AAID-PSSA323%3E3.0.CO%3B2-6.

- [177] W.S.M. Werner, K. Glantschnig, C. Ambrosch-Draxl, Optical constants and inelastic electron-scattering data for 17 elemental metals, J. Phys. Chem. Ref. Data 38 (2009), 1013. http://link.aip.org/link/?JPR/38/1013/1.
- [178] P.B. Allen, Electron-phonon effects in the infrared properties of metals, Phys. Rev. B 3 (1971), 305, https://doi.org/10.1103/PhysRevB.3.305.
- [179] S.J. Youn, T.H. Rho, B.I. Min, K.S. Kim, Extended drude model analysis of noble metals, phys. Stat. sol. (b) 244 (2007), 1354, https://doi.org/10.1002/pssb.200642097.
- [180] K.H. Bennemann, Ultrafast dynamics in solids, J. Phys.: Condens. Matter 16 (2004), R995. http://stacks.iop.org/0953-8984/16/i=30/a=R01.
- [181] G. Cisneros, J.S. Helman, Phonon contribution to the frequency-dependent part of the relaxation time involved in the intraband optical conductivity of noble metals, Phys. Rev. B 25 (1982), 6504, https://doi.org/10.1103/PhysRevB.25.6504.
- [182] M.S. Wismer, S.Y. Kruchinin, M. Ciappina, M.I. Stockman, V.S. Yakovlev, Strong-field resonant dynamics in semiconductors, Phys. Rev. Lett. 116 (2016), 197401, https://doi.org/10.1103/PhysRevLett.116.197401.
- [183] S.Y. Kruchinin, F. Krausz, V.S. Yakovlev, Colloquium: Strong-field phenomena in periodic systems, Rev. Mod. Phys. 90 (2018), 021002. https://link.aps.org/doi/10.1103/RevModPhys.90.021002.
- [184] C. Schmidt, J. Bühler, A.-C. Heinrich, J. Allerbeck, R. Podzimski, D. Berghoff, T. Meier, W.G. Schmidt, C. Reichl, W. Wegscheider, D. Brida, A. Leitenstorfer, Signatures of transient Wannier-Stark localization in bulk gallium arsenide, Nat. Commun. 9 (1) (2018), https://doi.org/10.1038/s41467-018-05229-x.
- [185] F. Langer, C.P. Schmid, S. Schlauderer, M. Gmitra, J. Fabian, P. Nagler, C. Schüller, T. Korn, P.G. Hawkins, J.T. Steiner, U. Huttner, S.W. Koch, M. Kira, R. Huber, Lightwave valleytronics in a monolayer of tungsten diselenide, Nature 557 (7703) (2018) 76–80, https://doi.org/10.1038/s41586-018-0013-6.
- [186] J. Reimann, S. Schlauderer, C.P. Schmid, F. Langer, S. Baierl, K.A. Kokh, O.E. Tereshchenko, A. Kimura, C. Lange, J. Güdde, U. Höfer, R. Huber, Subcycle observation of lightwave-driven Dirac currents in a topological surface band, Nature 562 (7727) (2018) 396–400, https://doi.org/10.1038/s41586-018-0544-x
- [187] R.T. Beach, R.W. Christy, Electron-electron scattering in the intraband optical conductivity of Cu, Ag, and Au, Phys. Rev. B 16 (1977), 5277, https://doi.org/10.1103/PhysRevB.16.5277.
- [188] S. Tan, A. Argondizzo, C. Wang, X. Cui, H. Petek, Ultrafast multiphoton thermionic photoemission from graphite, Phys. Rev. X 7 (2017), 011004, https://doi. org/10.1103/PhysRevX.7.011004.
- [189] D.A. Shirley, High-resolution X-ray photoemission spectrum of the valence bands of gold, Phys. Rev. B 5 (1972), 4709, https://doi.org/10.1103/ PhysRevB.5.4709.
- [190] N. Pontius, V. Sametoglu, H. Petek, Simulation of two-photon photoemission from the bulk sp-bands of Ag(111), Phys. Rev. B 72 (2005), 115105. http://link.aps.org/abstract/PRB/v72/e115105.
- [191] Z. Yuan, S. Gao, Landau damping and lifetime oscillation of surface plasmons in metallic thin films studied in a jellium slab model, Surf. Sci. 602 (2008), 460. http://www.sciencedirect.com/science/article/B6TVX-4R1MDY2-2/2/a7dfa9f8d926ac7e38be23a9f277f7fe.
- [192] X. Li, D. Xiao, Z. Zhang, Landau damping of quantum plasmons in metal nanostructures, New J. Phys. 15 (2013), 023011. http://stacks.iop.org/1367-2630/15/i=2/a=023011.
- [193] J. B. Khurgin and G. Sun, Quantum plasmonics (Springer, 2016), Vol. 185, pp. 303.
- [194] N. Thakkar, N.P. Montoni, C. Cherqui, D.J. Masiello, Plasmonic landau damping in active environments, Phys. Rev. B 97 (2018), 121403, https://doi.org/10.1103/PhysRevB.97.121403.
- [195] D. Pines P. Noziéres The theory of quantum liquids (Benjamin Vol. I 1966 New York and Amsterdam.
- [196] A. Kawabata, R. Kubo, Electronic properties of fine metallic particles. II. plasma resonance absorption, J. Phys. Soc. Jap. 21 (1966), 1765.
- [197] P. Dombi, et al., Strong-field nano-optics, Rev. Mod. Phys. 92 (2020), 025003, https://doi.org/10.1103/RevModPhys.92.025003.
- [198] S. Ogawa, H. Nagano, H. Petek, Optical intersubband transitions and femtosecond dynamics in Ag /Fe(100) quantum wells, Phys. Rev. Lett. 88 (2002), 116801. http://link.aps.org/abstract/PRL/v88/e116801.
- [199] R. Sundararaman, P. Narang, A.S. Jermyn, W.A. Goddard III, H.A. Atwater, Theoretical predictions for hot-carrier generation from surface plasmon decay, Nat. Commun. 5 (2014), 1, https://doi.org/10.1038/ncomms6788.
- [200] A.M. Brown, R. Sundararaman, P. Narang, W.A. Goddard, H.A. Atwater, Nonradiative plasmon decay and hot carrier dynamics: effects of phonons, surfaces, and geometry, ACS Nano 10 (1) (2016) 957–966.
- [201] P. Narang, R. Sundararaman, H.A. Atwater, Plasmonic hot carrier dynamics in solid-state and chemical systems for energy conversion, Nanophotonics 5 (2016), 96. https://www.degruyter.com/view/journals/nanoph/5/1/article-p96.xml.
- [202] J.A. Sobota, Y. He, Z.-X. Shen, Angle-resolved photoemission studies of quantum materials, Rev. Mod. Phys. 93 (2021), 025006, https://doi.org/10.1103/ RevModPhys.93.025006.
- [203] J. Lehmann, M. Merschdorf, W. Pfeiffer, A. Thon, S. Voll, G. Gerber, Surface plasmon dynamics in silver nanoparticles studied by femtosecond time-resolved photoemission, Phys. Rev. Lett. 85 (2000), https://doi.org/10.1103/PhysRevLett.85.2921.
- [204] H. Petek, Photoexcitation of adsorbates on metal Surfaces: one-step or three-step, J. Chem. Phys. 137 (2012), 091704, https://doi.org/10.1063/1.4746801.
- [205] K. Wu, J. Chen, J.R. McBride, T. Lian, Efficient hot-electron transfer by a plasmon-induced interfacial charge-transfer transition, Science 349 (2015), 632. http://www.sciencemag.org/content/349/6248/632.abstract.
- [206] K. Ishioka, M. Hase, M. Kitajima, L. Wirtz, A. Rubio, H. Petek, Ultrafast electron-phonon decoupling in graphite, Phys. Rev. B 77 (2008), 121402. http://link.aps.org/abstract/PRB/v77/e121402.
- [207] G. Rohde, et al., Ultrafast formation of a fermi-dirac distributed electron gas, Phys. Rev. Lett. 121 (2018), 256401, https://doi.org/10.1103/ PhysRevLett.121.256401.
- [208] J.J. Quinn, Range of excited electrons in metals, Phys. Rev. 126 (1962), 1453. http://link.aps.org/abstract/PR/v126/p1453.
- [209] P.M. Echenique, J.M. Pitarke, E.V. Chulkov, A. Rubio, Theory of inelastic lifetimes of low-energy electrons in metals, Chem. Phys. 251 (1) (2000). https://www.sciencedirect.com/science/article/pii/S0301010499003134.
- [210] G. Moos, C. Gahl, R. Fasel, M. Wolf, T. Hertel, Anisotropy of quasiparticle lifetimes and the role of disorder in graphite from ultrafast time-resolved photoemission spectroscopy, Phys. Rev. Lett. 87 (2001), 267402. http://link.aps.org/abstract/PRL/v87/e267402.
- [211] V.M. Silkin, J. Zhao, F. Guinea, E.V. Chulkov, P.M. Echenique, H. Petek, Image potential states in graphene, Phys. Rev. B 80 (2009), 121408. http://link.aps. org/abstract/PRB/v80/e121408.
- [212] C.M. Horowitz, L.A. Constantin, C.R. Proetto, J.M. Pitarke, Position-dependent exact-exchange energy for slabs and semi-infinite jellium, Phys. Rev. B 80 (2009), 235101, https://doi.org/10.1103/PhysRevB.80.235101.
- [213] C.W. Hsu, B. Zhen, A.D. Stone, J.D. Joannopoulos, M. Soljačić, Bound states in the continuum, Nat. Rev. Mater. 1 (2016), 16048, https://doi.org/10.1038/
- [214] T.-S. Choy, J. Naset, S. Hershfield, and C. Stanton, The Fermi surface data base, (Florida State University) http://www.phys.ufl.edu/fermisurface/.
- [215] E.V. Chulkov, V.M. Silkin, P.M. Echenique, Image potential states on metal surfaces: Binding energies and wave functions, Surf. Sci. 437 (1999), 330. http://www.scopus.com/scopus/inward/record.url?eid=2-s2.0-0032669639&partnerID=40&rel=R5.6.0.
- [216] M. Bernardi, J. Mustafa, J.B. Neaton, S.G. Louie, Theory and computation of hot carriers generated by surface plasmon polaritons in noble metals, Nat. Commun. 6 (2015), https://doi.org/10.1038/ncomms8044.
- [217] A. Winkelmann, V. Sametoglu, J. Zhao, A. Kubo, H. Petek, Angle-dependent study of a direct optical transition in the sp bands of Ag(111) by one- and two-photon photoemission, Phys. Rev. B 76 (2007), 195428. http://link.aps.org/abstract/PRB/v76/e195428.
- [218] T. Fauster, W. Steinmann, in: Photonic probes of surfaces, North-Holland, Amsterdam, 1995, 347.
- [219] F. Reinert, G. Nicolay, S. Schmidt, D. Ehm, S. Hüfner, Direct measurements of the L-gap surface states on the (111) face of noble metals by photoelectron spectroscopy, Phys. Rev. B 63 (2001), 115415. http://link.aps.org/abstract/PRB/v63/e115415.
- [220] M. Marks, C.H. Schwalb, K. Schubert, J. Güdde, U. Höfer, Quantum-beat spectroscopy of image-potential resonances, Phys. Rev. B 84 (2011), 245402. http://link.aps.org/doi/10.1103/PhysRevB.84.245402.

- [221] X. Cui, C. Wang, A. Argondizzo, S. Garrett-Roe, B. Gumhalter, H. Petek, Transient excitons at metal surfaces, Nat. Phys. 10 (7) (2014) 505–509, https://doi.org/10.1038/nphys2981.
- [222] V.M. Silkin, P. Lazić, N. Došlić, H. Petek, B. Gumhalter, Ultrafast electronic response of Ag(111) and Cu(111) surfaces: From early excitonic transients to saturated image potential, Phys. Rev. B 92 (2015), 155405, https://doi.org/10.1103/PhysRevB.92.155405.
- [223] P.M. Echenique, J.B. Pendry, Theory of image states at metal surfaces, Prog. Surf. Sci. 32 (1990), 111.
- [224] T. Miller, W.E. McMahon, T.C. Chiang, Interference between bulk and surface photoemission transitions in Ag(111), Phys. Rev. Lett. 77 (1996), 1167. http://link.aps.org/abstract/PRL/v77/p1167.
- [225] M. Marks, Ph. D. Thesis, Philipps-Universitaet Marburg, 2012.
- [226] F. Himpsel, J. Ortega, Electronic structure of Cu(100), Ag(100), Au(100), and Cu₃Au(100) from inverse photoemission, Phys. Rev. B 46 (1992), 9719. http://link.aps.org/doi/10.1103/PhysRevB.46.9719.
- [227] T. Eul, J. Braun, B. Stadtmüller, H. Ebert, M. Aeschlimann, Spectroscopic evidence for a new type of surface resonance at noble-metal surfaces, Phys. Rev. Lett. 127 (2021), 196405, https://doi.org/10.1103/PhysRevLett.127.196405.
- [228] T. Eul, E. Prinz, M. Hartelt, B. Frisch, M. Aeschlimann, B. Stadtmüller, Coherent response of the electronic system driven by non-interfering laser pulses, Nat. Commun. 13 (2022), 3324. https://doi.org/10.1038/s41467-022-30768-9.
- [229] M. Keunecke, et al., Electromagnetic dressing of the electron energy spectrum of Au(111) at high momenta, Phys. Rev. B 102 (2020), 161403, https://doi.org/10.1103/PhysRevB.102.161403.
- [230] D. Schmitt, J.P. Bange, W. Bennecke, AbdulAziz AlMutairi, G. Meneghini, K. Watanabe, T. Taniguchi, D. Steil, D.R. Luke, R.T. Weitz, S. Steil, G.S.M. Jansen, S. Brem, E. Malic, S. Hofmann, M. Reutzel, S. Mathias, Formation of moiré interlayer excitons in space and time, Nature 608 (7923) (2022) 499–503, https://doi.org/10.1038/s41586-022-04977-7.
- [231] J.C. Phillips, Further evidence for collective resonances in monovalent metals, Phys. Rev. 137 (1965), A1835, https://doi.org/10.1103/PhysRev.137.A1835.
- [232] K. Giesen, F. Hage, F.J. Himpsel, H.J. Riess, W. Steinmann, Two-photon photoemission via image-potential states, Phys. Rev. Lett. 55 (1985), 300, https://doi.org/10.1103/PhysRevLett.55.300.
- [233] N.B. Gornyi, E.N. Makarova, Detection of the plasmon photoeffect of alkali metals in photoelectron energy distribution curves, Sov. Phys. J. 16 (10) (1973) 1406–1410, https://doi.org/10.1007/BF00894413.
- [234] W. Steinmann, Two-photon photoemission spectroscopy of electronic states at metal surfaces, Phys. Status Solidi (b) 192 (1995), 339, https://doi.org/10.1002/pssb.2221920210.
- [235] V.U. Nazarov, V.M. Silkin, E.E. Krasovskii, Role of the kinematics of probing electrons in electron energy-loss spectroscopy of solid surfaces, Phys. Rev. B 93 (2016), 035403, https://doi.org/10.1103/PhysRevB.93.035403.
- [236] U. Höfer, P.M. Echenique, Resolubility of image-potential resonances, Surf. Sci. 643 (2016), 203, https://doi.org/10.1016/j.susc.2015.07.019.
- [237] F. Moresco, M. Rocca, V. Zielasek, T. Hildebrandt, M. Henzler, ELS-LEED study of electronic excitations on Ag(110) and Ag(111), Surf. Sci. 388 (1997), 24. http://www.sciencedirect.com/science/article/pii/S0039602897002781.
- [238] B. Gumhalter, Stages of hot electron dynamics in multiexcitation processes at surfaces: general properties and benchmark examples, Prog. Surf. Sci. 87 (2012), 163. http://www.sciencedirect.com/science/article/pii/S0079681612000135.
- [239] R. Rosei, C.H. Culp, J.H. Weaver, Temperature modulation of the optical transitions involving the Fermi surface in Ag: experimental, Phys. Rev. B 10 (1974), 484, https://doi.org/10.1103/PhysRevB.10.484.
- [240] Y. Borensztein, Investigation of nonlocal electromagnetic phenomena in thin silver films near the plasma frequency, J. Opt. Soc. Am. 73 (1983), 80. http://www.osapublishing.org/abstract.cfm?URI=josa-73-1-80.
- [241] J.S. Zhou, et al., Unraveling intrinsic correlation effects with angle-resolved photoemission spectroscopy, Proceed. Natl. Acad. Sci. 117 (2020), 28596. https://www.pnas.org/doi/abs/10.1073/pnas.2012625117.
- [242] A. Bostwick, F. Speck, T. Seyller, K. Horn, M. Polini, R. Asgari, A.H. MacDonald, E. Rotenberg, Observation of plasmarons in quasi-freestanding doped graphene, Science 328 (2010), 999. http://www.sciencemag.org/cgi/content/abstract/328/5981/999.
- [243] M. Jablan, M. Soljacic, H. Buljan, Plasmons in graphene: fundamental properties and potential applications, Proc. IEEE 101 (2013), 1689, https://doi.org/10.1109/JPROC.2013.2260115.
- [244] J.S. Zhou, M. Gatti, J.J. Kas, J.J. Rehr, L. Reining, Cumulant Green's function calculations of plasmon satellites in bulk sodium: influence of screening and the crystal environment, Phys. Rev. B 97 (2018), 035137, https://doi.org/10.1103/PhysRevB.97.035137.
- [245] W. R. Marry Jr., Ph. D. Thesis, University of California at Berkeley, 1992.
- [246] Y. Borensztein, A. Tadjeddine, W.L. Mochan, J. Tarriba, R.G. Barrera, Optical anisotropies of Ag single crystals, Thin Solid Films 233 (1993), 24. http://www.sciencedirect.com/science/article/pii/0040609093900548.
- [247] Y. Sonoda, Electronic states of Cu(110) investigated with angle-resolved two-photon photoemission spectroscopy, Phys. Rev. B 83 (2011), 245410, https://doi.org/10.1103/PhysRevB.83.245410.
- [248] H.J. Levinson, E.W. Plummer, P.J. Feibelman, Effects on photoemission of the spatially varying photon field at a metal surface, Phys. Rev. Lett. 43 (1979), 952, https://doi.org/10.1103/PhysRevLett.43.952.
- [249] R.A. Bartynski, E. Jensen, T. Gustafsson, E.W. Plummer, Angle-resolved photoemission investigation of the electronic structure of Be: surface states, Phys. Rev. B 32 (1985), 1921, https://doi.org/10.1103/PhysRevB.32.1921.
- [250] S.R. Barman, P. Häberle, K. Horn, Collective and single-particle excitations in the photoyield spectrum of Al, Phys. Rev. B 58 (1998), R4285, https://doi.org/10.1103/PhysRevB.58.R4285.
- [251] M. Shibuta, K. Yamamoto, T. Ohta, T. Inoue, K. Mizoguchi, M. Nakaya, T. Eguchi, A. Nakajima, Confined hot electron relaxation at the molecular heterointerface of the size-selected plasmonic noble metal nanocluster and layered C₆₀, ACS Nano 15 (1) (2021) 1199–1209, https://doi.org/10.1021/ acsnano.0c08248.
- [252] M. Hartelt, P.N. Terekhin, T. Eul, A.-K. Mahro, B. Frisch, E. Prinz, B. Rethfeld, B. Stadtmüller, M. Aeschlimann, Energy and momentum distribution of surface plasmon-induced hot carriers isolated via spatiotemporal separation, ACS Nano 15 (12) (2021) 19559–19569, https://doi.org/10.1021/acsnano.1c06586.
- [253] P. Dreher, D. Janoschka, A. Neuhaus, B. Frank, H. Giessen, M. Horn-von Hoegen, F.-J. Meyer zu Heringdorf, Quantitative determination of the electric field strength in a plasmon focus from ponderomotive energy shifts, Nanophotonics 11 (16) (2022) 3687–3694, https://doi.org/10.1515/nanoph-2022-0284.
- [254] P. Dreher, D. Janoschka, B. Frank, H. Giessen, F.-J. Meyer, zu, Heringdorf, Focused surface plasmon polaritons coherently couple to electronic states in above-threshold electron emission, Commun. Phys. 6 (2023), 15, https://doi.org/10.1038/s42005-023-01128-w.
- [255] M.J. Weida, S. Ogawa, H. Nagano, H. Petek, Ultrafast interferometric pump-probe correlation measurements in systems with broadened bands or continua, J. Opt. Soc. Am. B 17 (2000), 1443. http://www.opticsinfobase.org/josab/abstract.cfm?URI=josab-17-8-1443.
- [256] H. Petek, Y. Dai, A. Ghosh, A. Li, Z. Zhou, M. Reutzel, S. Yang, and C.-B. Huang, in *Emerging Trends in Chemical Applications of Lasers* (American Chemical Society, 2021), pp. 153.
- [257] J. Mauritsson, et al., Attosecond electron spectroscopy using a novel interferometric pump-probe technique, Phys. Rev. Lett. 105 (2010), 053001, https://doi.org/10.1103/PhysRevLett.105.053001.
- [258] H. C. Strauch, M. S. thesis, University of Göttingen, 2022.
- [259] M. Rocca, Low-energy EELS investigation of surface electronic excitations on metals, Surf. Sci. Rep. 22 (1) (1995). http://www.sciencedirect.com/science/article/pii/0167572995000046.
- [260] M. Rocca, Y. Li, F. Buatier de Mongeot, U. Valbusa, Surface plasmon dispersion and damping on Ag(111), Phys. Rev. B 52 (1995), 14947, https://doi.org/10.1103/PhysRevB.52.14947.
- [261] L. Yibing, A.C. Levi, M. Rocca, Anisotropy of surface plasmons in metals, Surf. Sci. 336 (1995), 371. http://www.sciencedirect.com/science/article/pii/ 003960289500520X.

- [262] A. Politano, G. Chiarello, The influence of electron confinement, quantum size effects, and film morphology on the dispersion and the damping of plasmonic modes in Ag and Au thin films, Prog. Surf. Sci. 90 (2015), 144. http://www.sciencedirect.com/science/article/pii/S007968161400032X.
- [263] F. Bisio, A. Winkelmann, C.-T. Chiang, H. Petek, J. Kirschner, Band structure effects in above threshold photoemission, J. Phys. Condens. Matter 23 (2011), 485002. http://stacks.iop.org/0953-8984/23/i=48/a=485002.
- [264] F. J. Himpsel and I. Lindau, (Wiley-VCH, Weinheim, 2009), pp. 285.
- [265] A. Li, Ph. D. Thesis, University of Pittsburgh, 2022.
- [266] G. Ferrini, C. Giannetti, G. Galimberti, S. Pagliara, D. Fausti, F. Banfi, F. Parmigiani, Violation of the electric-dipole selection rules in indirect multiphoton excitation of image-potential states on Ag(100), Phys. Rev. Lett. 92 (2004), 256802, https://doi.org/10.1103/PhysRevLett.92.256802.
- [267] S. Pagliara, et al., Nature of the surface states at the single-layer graphene/Cu(111) and graphene/polycrystalline-Cu interfaces, Phy. Rev. B 91 (2015), 195440, https://doi.org/10.1103/PhysRevB.91.195440.
- [268] Y.H. Wang, H. Steinberg, P. Jarillo-Herrero, N. Gedik, Observation of floquet-bloch states on the surface of a topological insulator, Science 342 (2013), 453. http://www.sciencemag.org/content/342/6157/453.abstract.
- [269] B. Gumhalter, in: Encyclopedia of interfacial chemistry, Elsevier, Oxford, 2018, 668.
- [270] R. Li, J. Wang, X.-L. Qi, S.-C. Zhang, Dynamical axion field in topological magnetic insulators, Nat. Phys. 6 (4) (2010) 284–288, https://doi.org/10.1038/nphys1534.
- [271] K.Y. Bliokh, Y.S. Kivshar, F. Nori, Magnetoelectric effects in local light-matter interactions, Phys. Rev. Lett. 113 (2014), 033601, https://doi.org/10.1103/PhysRevLett.113.033601.
- [272] C. Caloz, A. Alù, S. Tretyakov, D. Sounas, K. Achouri, Z.-L. Deck-Léger, Electromagnetic nonreciprocity, Phys. Rev. Appl. 10 (2018), 047001, https://doi.org/10.1103/PhysRevApplied.10.047001.